Seismic Performance Assessment of High Asphalt Concrete Core Rockfill Dam Considering Shorter Duration and Longer Duration

benbo sun
Tianjin University
Mingjiang Deng
Xinjiang Ertix River Basin Development and Construction Management Bureau
Sherong Zhang
Tianjin University
Chao Wang (janson126@163.com)
Tianjin university https://orcid.org/0000-0003-1853-2833
Guojin Zhu
Kunming Engineering Corporation Limited

Research Article

Keywords: Integrated duration, Asphalt concrete core rockfill dam, Fragility analysis, Performance level, Multiple stripe analysis

Posted Date: June 1st, 2021

DOI: https://doi.org/10.21203/rs.3.rs-501314/v1

Version of Record: A version of this preprint was published at Structures on May 1st, 2022. See the published version at https://doi.org/10.1016/j.istruc.2022.03.040.

Seismic performance assessment of high asphalt concrete core rockfill dam considering shorter duration and longer duration

Benbo Sun[a,b,c]·Mingjiang Deng[a,d]·Sherong Zhang[a,b,c]·Chao Wang[a,b,c*]·Guojin Zhu[e]

a State Key Laboratory of Hydraulic Engineering Simulation and Safety, Tianjin University, Tianjin 300350, China

b Key Laboratory of Earthquake Engineering Simulation and Seismic Resilience of China Earthquake Administration, Tianjin 300350, China;

c School of Civil Engineering, Tianjin University, Tianjin 300350, China

d Xinjiang Ertix River Basin Development and Construction Management Bureau, Urumqi 830000, China

e POWERCHINA Kunming Engineering Corporation Limited, Kunming 650051, China

Abstract

Current research trends in seismic frequent regions aim at developing the appropriate performance – based design approach for high asphalt concrete core rockfill dams (ACCRDs). Under intense ground motions (GMs), the seismic performance of dams depends on seismological characteristics mainly containing the frequency, amplitude, and duration. Recently, the characteristic of frequency and amplitude of GMs which can trigger severe damages to the dams has been accepted and incorporated into the seismic design codes in most countries. As one of the key characteristics of earthquakes, the duration of strong GMs also should be fully understood in order to carry out more

reasonable performance – based design approach of dams. This paper explores the effect of the duration of strong GMs, investing the seismic performance of high ACCRDs by employing integrated duration concept, which can reflect the duration of all components of GMs. The high ACCRD was built in the commercial software ABAQUS considering the dam-reservoir-foundation interaction systems. Additionally, the coupling multiple stripe analysis and maximum likelihood estimate method are used to generate seismic fragility curves for the dam according to two damage indicators. Findings from this study revealed that the longer duration GMs can give rise to higher probability of exceedance (POE) of the dam than shorter duration. It is recommended that in the work of the current seismic design and seismic performance evaluate, the effects of GM duration in addition to frequency and amplitude should be considered.

Keywords: Integrated duration; Asphalt concrete core rockfill dam; Fragility analysis; Performance level; Multiple stripe analysis

1. Introduction

High dams are regarded as critical components of a nation's lifeline engineering, which can effectively alleviate the contradiction between water supply and demand. Over the past few decades, the rapidly development of water resource has witnessed a boom and a larger number of embankment dams has been constructed all over the word because of their low cost, rapid, and adaptability. Recently, owing to the optimization and improvement of downstream water resources, the development and construction of high dams are gradually turning to the upstream of each watershed. High asphalt concrete core rockfill dams (ACCRDs) has attracted the interest of the world's dam designers in

upstream water resource development (Wang et al., 2010; Wang and Höeg, 2016). The mains reason for this is that the ACCRDs are situated in regions with variable climatic conditions and complex geological environment, or in areas with a shortage of natural earth core material. In light of the vulnerability of ACCRDs to strong ground motions (GMs), evaluating their seismic performance and safety is of obvious practical importance in dam construction and operation (Baziar et al., 2009). Currently, the prediction of the seismic performance of ACCRDs under GM excitation is still far behind concrete dams or other types of embankment dams.

Earthquake disaster that have frequently occurred in recent years, containing those in Sumatra, Indonesia (Mw 9.1, 2004), Wenchuan, China (Mw 7.9, 2008), Maule, Chile (Mw8.8, 2010), Tohoku, Japan (Mw 9.0, 2011), continue to remind us that strong GMs may trigger devastating high dam – break floods and further influence large regions downstream. The most significant particularly features of GMs are propagation path of seismic waves, spatial site conditions, source mechanism, ground motion duration (GMD), frequency and amplitude, each of which may plays a critical part in the seismic performance assessment. Generally, the characteristic of amplitude, which is one of effective engineering parameters on seismic performance assessment of structures, is illustrated by the peak ground displacement (PGD), the peak ground velocity (PGV) and the peak ground acceleration (PGA). Moreover, the Fourier spectrum of the GM is usually employed to reveal the frequency content. Conversely, present seismic design code and analysis methodology do not directly or indirectly consider the impact of GMD on the seismic performance of high ACCRDs. Besides, the length of the spatial distribution of GMDs is influenced by defining methods, site conditions, basin effects and rupture directivity (see Fig. 1) according to the record of Wenchuan earthquake. That is to say, if the

significant particularly features of the earthquake disaster are different, the high ACCRDs may encounter different durations of GMs during its life cycle. However, the seismic performance assessment of high ACCRDs under shorter duration motions and longer duration motions have not been verified.

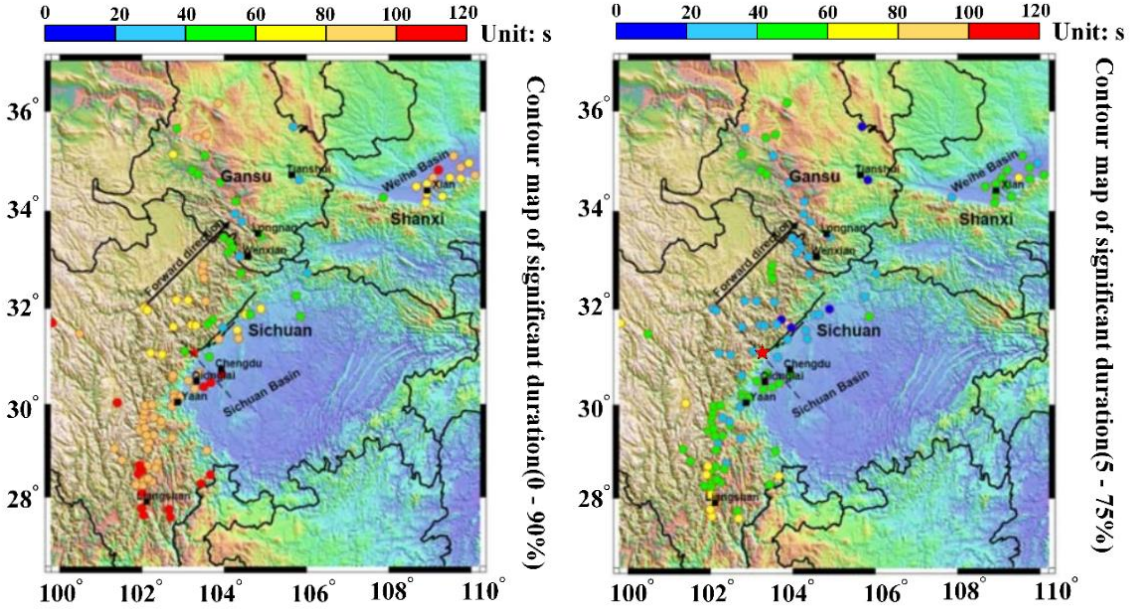

Fig. 1. Spatial distribution of significant duration recorded from Wenchuan earthquake (Mw7.9, 2008). (a) 0-90% significant duration; (b) 5-75% significant duration.

The effect of strong GMD on structural performance remains a rising controversial topic. It is well-known that GMD have a significant impact on some types of earthquake damage, such as containing high dams (Zhang et al., 2013), bridges (Ou et al., 2014), and liquefaction (Green and Terri, 2005). Yet, several investigations on the influence of GMD on the structural response have shown that the GMD have insignificant effects on structural response. For example, Kitayama and Constantinou (2020) concluded that the peak isolator resultant displacement is no stronger correlation to the GMD. The relationship observed between structural response and GMD cannot be recognized uniform (Raghunandan and Lie, 2013). In other words, a large number of in-depth studies are needed to reveal

the influence of GMD on the structural performance for different types of structures. On the other hand, some previous studies (Bommer and Martinez-Pereira, 1999; Green and Terri, 2005; Kitayama and Constantinou, 2020; Ou et al., 2014; Raghunandan and Liel, 2013; Trifunac and Brady, 1975; Zhang et al., 2013) on the impact of GMD on the structural performance only considering the one directional GMD. Nevertheless, the duration of GMs in one direction does not fully reflect the difference of duration in multi-direction. So far, it is worth noting that the definition of 30 different GMDs which does not clearly consensus on the multi-direction of duration of GMs. Very recently, to bridge the gap between multi-direction of GMs and duration employed for dynamic analysis, Wang et al. (2015) proposed a new duration concept of integrated duration (ID) to explain the duration component contributions of GMs in multi-direction. With the definition of ID, they reveal that the longer duration can cause greater damage cracks for Koyna concrete dam. Because of the randomness of earthquake disasters, the multi-direction of GMs have been recognized to easily trigger severe damage for high dams. Understanding the effect of multi-direction of GMD on the seismic performance assessment of high ACCRDs will bring the engineer one key step closer to decreasing the dam break risk.

Inspired by the above considerations, critical knowledge gaps exist in understanding and quantifying the impact of GMD on seismic performance of high ACCRDs. Therefore, the main objective of this paper is to highlight the significance of GMD for seismic performance assessment of high ACCRDs considering the shorter duration and longer duration. This paper consists of six major sections as follows. The basics concept and characteristic of ID is briefly reviewed in Section 2. In addition, to achieve this investigation, 30 short - and 16 long - durations of as-recorded GMs are selected in Section 2, and the distribution of the GMD generated spectrally equivalent methodology

97 are provided. The framework of seismic performance assessment is illustrated using the multiple stripe
98 analysis (MSA) and maximum likelihood estimate (MLE) with different seismic performance indices
99 in Section 3. In Section 4, the finite element (FE) numerical model for the high ACCRD is illustrated.
100 The seismic fragility analysis (FR) of the high ACCRD is discussed using the MSA - MLE with
101 different seismic performance indices in Section 5. Finally, summaries and conclusions follow in
102 Section 6.

103 **2. Integrated duration and ground motion database**

104 Although various definitions for GMD have been proposed to reveal the correlation between
105 GMD and the seismic performance of structures, there is still no universally recognized scientific
106 measure criterion of GMD since time history length of the accelerogram record may significantly
107 depend up on the recording device and structural performance. Among these widely differing measures,
108 the most generally applied scientific measure criterions for strong GMD can be characterized by four
109 measures including: bracketed duration (T_B) (Bolt, 1973), uniform duration (T_U) (Bommer et al., 2009),
110 significant duration (SD) (T_S) (Trifunac and Brady, 1975) and effective duration (T_E) (Bommer and
111 Martinez-Pereira, 1999). Apparently, all the aforementioned measures of GMD is generally used to
112 illustrating the duration of GMs in one direction. To be specific, the multi-direction incident seismic
113 waves brings about challenge for decouple the effect of GMD in different directions. According to the
114 concept of ID, the SD of different directions of GMs are selected as the basic component. The SD is
115 regard as an effective measure representing the duration of GMs by a relative scientific criterion. In
116 addition, the Husid diagram is determined to be the time history of the seismic energy content scaled

to the total energy content (Trifunac and Brady, 1975), which satisfied the Eq. (1):

$$H(t)=\frac{\frac{\pi}{2g}\int_0^t a^2(t)dt}{I_0} \tag{1}$$

where $H(t)$ is the Husid diagram defined as a function of time t. a is the time history of accelerogram and g is the gravitational acceleration. The total Arias intensity, I_0, is obtained from Eq. (2):

$$I_0=\frac{\pi}{2g}\int_0^{T_{\max}} a^2(t)dt \tag{2}$$

where T_{Max} is the length of the time history of accelerogram. Fig. 2 illustrates the SD of an as-record strong GMs in different ranges of Arias intensity.

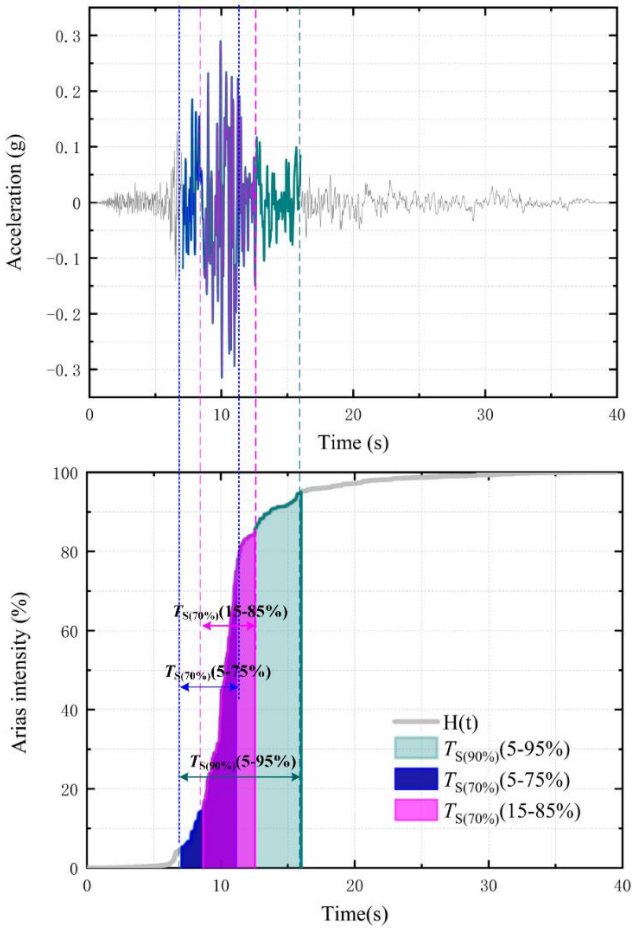

Fig. 2. The husid diagram of three SDs of an as-record accelerogram.

It can be seen from Fig. 2 and Eq. (2) that the SD can only properly express the duration of GM in single direction (horizontal or vertical component). On the contrary, the ID regards the Arias intensity in multi-directions as the weighting function, which is applied to weighted average the corresponding single direction duration to overcome the above shortcomings. Based on the work of Wang et al. (2015) the detailed formula of ID considering double directional GMs can be determined as follows:

$$T_I = \frac{T_S{}^H \times I_0^H + T_S{}^V \times I_0^V}{I_0^H + I_0^V} \tag{3}$$

where T_S^H and T_S^V denotes the GMDs in the horizontal and vertical directions, respectively. I_0^H and I_0^V respectively represent the horizontal Arias intensities and vertical Arias intensities of GMs. The $T_{S(70\%)}(5-75\%)$ which can be easily defined as the time gap between 5% and 75% of the Husid diagram, is selected to indicate GMDs in multi-directions, as depicted in Fig. 3.

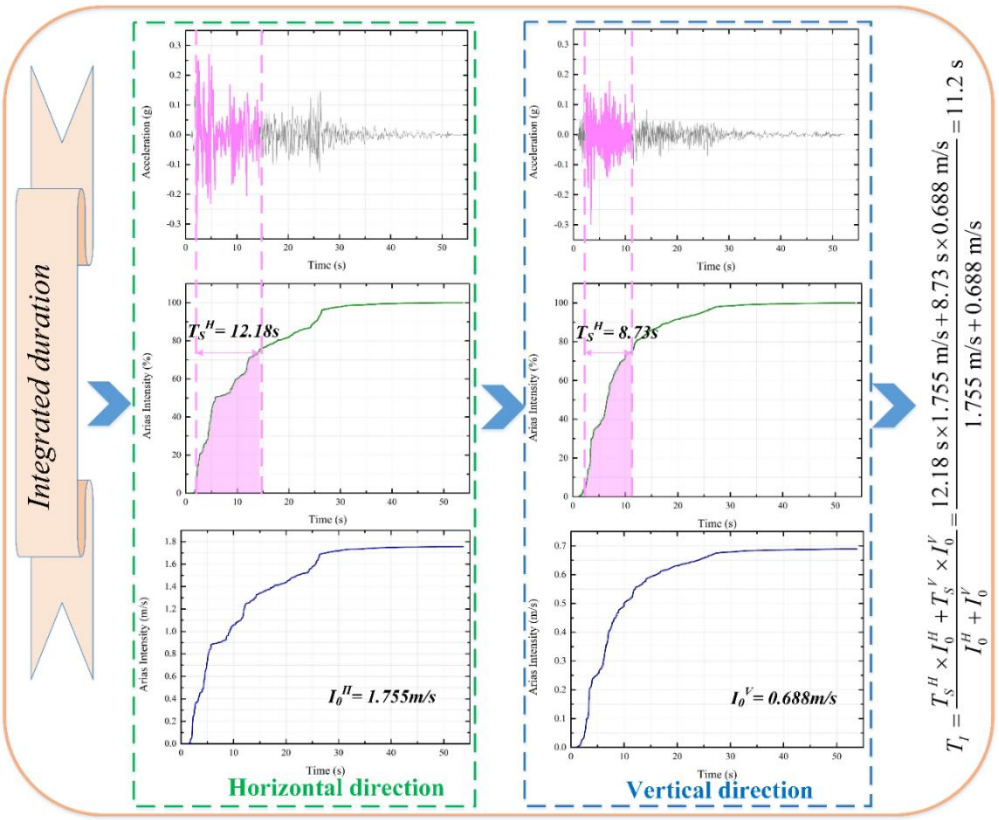

Fig. 3. Calculation progress of ID based on SD (5-75%).

To reveal the seismic performance of ACCRDs considering the shorter duration and longer duration effect, Forty - six bidirectional GMs are originated from the Pacific Earthquake Engineering Research center (PEER) strong database. For each of these short - duration bidirectional GMs, a corresponding long - duration bidirectional GMs with duration threshold longer than 25s (Barbosa et al., 2017), and having original spectral acceleration and matching spectral acceleration is determined. The detailed earthquake information is present in Table 1 and Table 2. On the other hand, it is crucial to avoid the impact of frequency, amplitude and other characteristics of GMs on the seismic performance assessment. All original GMs obtained PEER database are matched the target design spectrum by using time domain wavelet correction method to adjust the amplitude and shape of spectrum through the software of SeismoMatch. By doing so, the spectral acceleration of each bidirectional earthquake records is adjusted and scaled to have a good compatible with the target spectrum, reflecting that the influence of amplitude and shape of acceleration response spectrum can be minimized, as shown in Fig. 5. Figure. 6 illustrates the distribution of GMDs of matched GMs.

Table 1
List of short - duration database with two directions (matched records).

No.	Earthquake	Year	Station Name	Magnitude	Mechanism	Rrup (km)	Comp.	SD (5-75%) (s)	Arias (m/s)	ID (s)
1	Imperial Valley	1940	El Centro Array #9	6.95	strike slip	6.09	180	20.35	0.35	16.09
							up	9.31	0.22	
2	Imperial Valley	1951	El Centro Array #9	5.6	strike slip	25.24	0	12.22	0.06	15.61
							up	20.69	0.04	
3	Kern County	1952	Pasadena - CIT Athenaeum	7.36	Reverse	125.59	180	15.86	0.08	17.77
							up	20.32	0.06	
4	Imperial Valley	1953	El Centro Array #9	5.5	strike slip	15.64	0	6.4	0.03	7.92
							up	8.83	0.05	

5	Northern Calif	1954	Ferndale City Hall	6.5	strike slip	27.02	44	12.12	0.13	11.16
							up	9.07	0.06	
6	Hollister-01	1961	Hollister City Hall	5.6	strike slip	19.56	180	10.76	0.08	11.51
							up	12.7	0.05	
7	Parkfield	1966	Cholame - Shandon Array #12	6.19	strike slip	17.64	50	15.15	0.08	14.62
							down	14.1	0.08	
8	Borrego Mtn	1968	LA - Hollywood Stor FF	6.63	strike slip	222.42	90	8.72	0.04	7.34
							up	5.96	0.04	
9	Borrego Mtn	1968	San Onofre - So Cal Edison	6.63	strike slip	129.11	33	15	0.05	19.34
							up	22.96	0.06	
10	San Fernando	1971	Borrego Springs Fire Sta	6.61	Reverse	214.32	135	9.05	0.04	6.56
							down	4.08	0.04	
11	San Fernando	1971	Buena Vista - Taft	6.61	Reverse	112.52	90	10.59	0.04	13.65
							dowm	16.89	0.04	
12	San Fernando	1971	Cedar Springs_ Allen Ranch	6.61	Reverse	89.72	95	1.24	0.03	1.46
							down	1.69	0.03	
13	San Fernando	1971	Cholame - Shandon Array #2	6.61	Reverse	218.13	51	2.98	0.02	9.10
							down	11.55	0.05	
14	San Fernando	1971	Cholame - Shandon Array #8	6.61	Reverse	218.75	51	15.73	0.05	14.05
							down	11.95	0.04	
15	San Fernando	1971	Isabella Dam (Aux Abut)	6.61	Reverse	130.98	14	11.5	0.06	10.59
							down	9.45	0.05	
16	San Fernando	1971	LA - Hollywood Stor FF	6.61	Reverse	22.77	90	4.27	0.24	3.62
							up	2.75	0.18	
17	San Fernando	1971	Maricopa Array #1	6.61	Reverse	193.91	130	13.72	0.06	12.95
							down	12.02	0.05	
18	San Fernando	1971	Maricopa Array #2	6.61	Reverse	109.73	130	14.29	0.05	13.42
							down	12.335	0.04	
19	San Fernando	1971	Maricopa Array #3	6.61	Reverse	110.18	130	10.21	0.04	9.67
							down	9.14	0.04	
20	San Fernando	1971	Pacoima Dam (upper left abut)	6.61	Reverse	1.81	120	6	0.04	6.59
							up	7.18	0.04	
21	San Fernando	1971	Palmdale Fire Station	6.61	Reverse	28.99	120	10.23	0.18	10.96
							up	11.89	0.14	
22	San Fernando	1971	Pasadena - CIT Athenaeum	6.61	Reverse	25.47	0	7.32	0.10	7.91
							down	8.56	0.09	
23	San Fernando	1971	San Diego Gas & Electric	6.61	Reverse	205.77	0	25.03	0.05	24.73
							down	24.35	0.04	
24	San Fernando	1971	Santa Felita Dam (Outlet)	6.61	Reverse	24.87	172	16.1	0.16	16.56
							up	17.78	0.06	

25	San Fernando	1971	Wheeler Ridge - Ground	6.61	Reverse	70.23	90	9.96	0.03	18.01
							up	22.84	0.05	
26	San Fernando	1971	Whittier Narrows Dam	6.61	Reverse	39.45	143	9.73	0.10	10.09
							down	10.805	0.05	
27	Nicaragua	1972	Managua_ ESSO	5.2	strike slip	4.98	90	7.215	0.11	4.98
							down	2.53	0.10	
28	Point Mugu	1973	Port Hueneme	5.65	Reverse	17.71	180	5.735	0.07	4.52
							up	2.39	0.04	
29	Oroville	1975	Up & Down Cafe (OR1)	4.79	Normal	12.65	0	3.85	0.04	3.17
							down	2.255	0.03	
30	Oroville	1975	Oroville Airport	4.37	Normal Oblique	14.36	180	2.56	0.03	2.49
							down	2.415	0.03	

Table 2

List of long - duration database with two directions (matched records).

No.	Earthquake	Year	Station	Magnitude	Mechanism	Rrup (km)	Comp.	SD (5-75%) (s)	Arias (m/s)	ID (s)
1	Borrego Mtn	1968	El Centro Array #9	6.63	strike slip	45.66	180	25.54	0.24	25.64
							up	26.8	0.02	
2	Morgan Hill	1984	Fremont - Mission San Jose	6.19	strike slip	31.34	75	23.18	0.33	25.01
							up	26.85	0.33	
3	Landers	1992	Mission Creek Fault	7.28	strike slip	26.96	0	51.89	0.52	51.16
							up	50.46	0.54	
4	Chi-Chi	1999	CHY076	7.62	Reverse Oblique	42.15	E	64.43	1.23	54.16
							V	46.12	1.57	
5	Chi-Chi	1999	CHY082	7.62	Reverse Oblique	36.09	E	54.82	1.68	51.89
							V	42.24	0.51	
6	Chi-Chi	1999	KAU001	7.62	Reverse Oblique	44.93	N	34.82	1.12	43.44
							V	58.74	0.63	
7	Chi-Chi	1999	KAU077	7.62	Reverse Oblique	82.96	E	37.95	0.92	34.79
							V	32.09	1.08	
8	Chuetsu-oki	2007	AKTH02	6.8	Reverse	285.32	NS	22.835	0.81	37.43
							up	46.325	1.33	
9	Chuetsu-oki	2007	IWTH05	6.8	Reverse	271.78	NS	72.59	0.59	91.39
							up	102.83	0.97	
10	Iwate	2008	FKS025	6.9	Reverse	188.17	NS	37.37	0.25	42.04
							up	44.52	0.47	
11	Iwate	2008	FKSH05	6.9	Reverse	194.76	NS	43.3	0.41	56.80
							up	69.97	0.42	
12	Tottori	2000	MIEH05	6.61	strike slip	275.84	NS	41.055	1.17	41.65
							up	45.75	0.17	
13	Niigata	2004	IBR006	6.63	Reverse	171.21	NS	27.05	0.26	29.85
							up	34.15	0.17	

14	Niigata	2004	MYGH11	6.63	Reverse	243.44	NS	29.72	0.46	34.50
							up	39.38	0.45	
15	Niigata	2004	TYM003	6.63	Reverse	127.28	NS	24.07	0.25	28.37
							up	32.28	0.27	
16	Darfield	2010	TRCS	7	strike slip	95.85	E	20.955	0.60	25.82
							up	29.81	0.73	

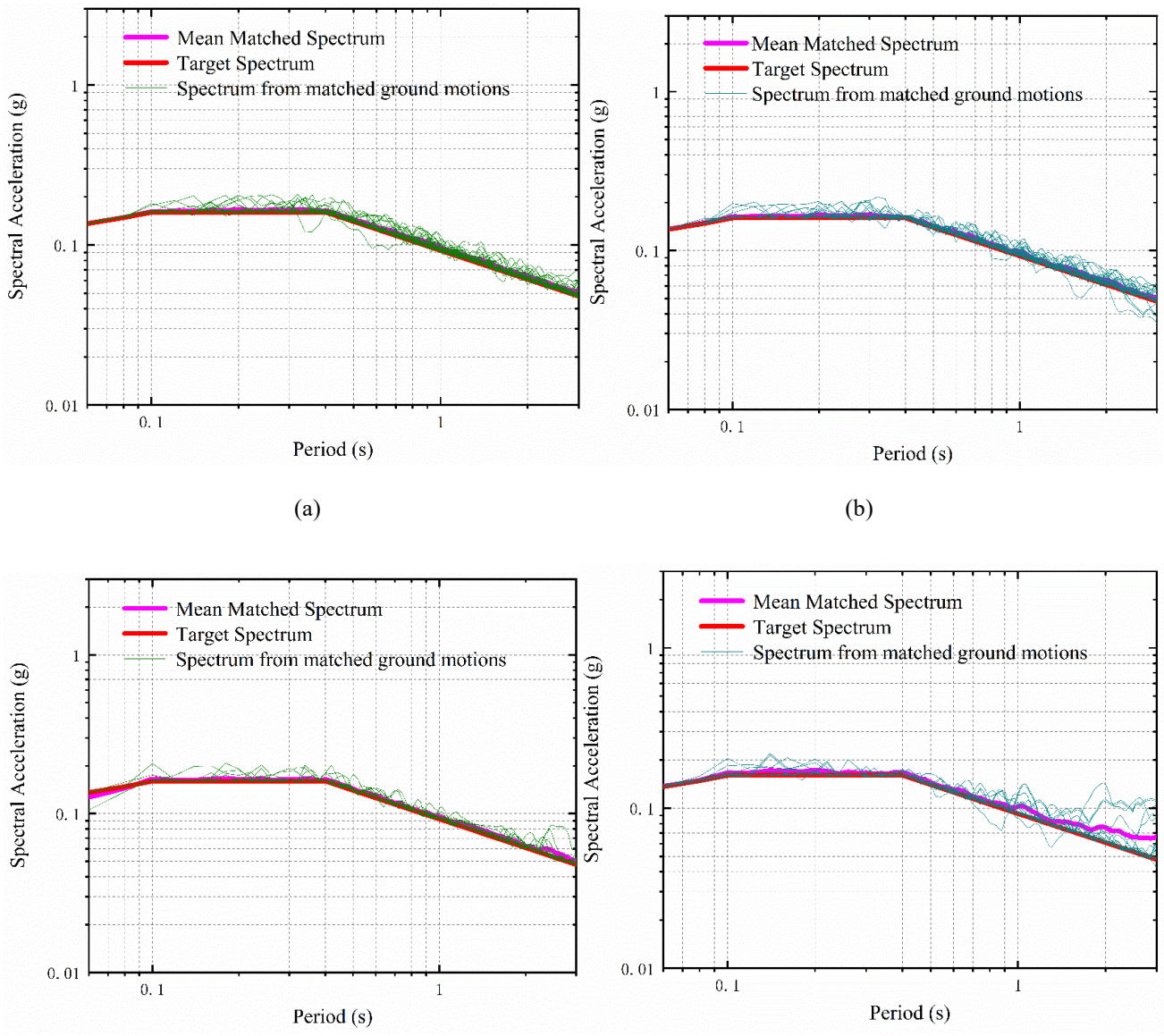

Fig. 4. Comparison of the adjusted response spectra of short - and long – duration GMs: (a) horizontal short – duration; (b) vertical direction short – duration; (c) horizontal long – duration; (b) vertical direction long – duration.

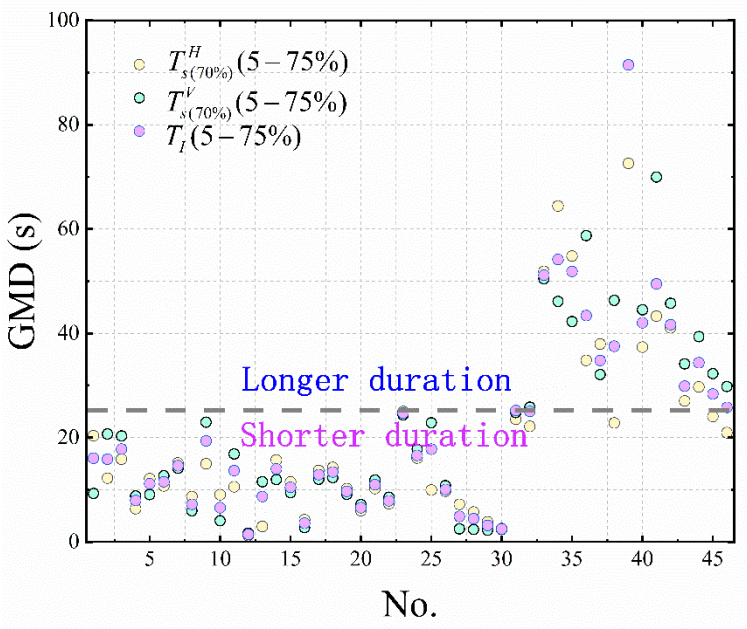

Fig. 5. Distribution of GMD in database after matching spectral acceleration.

3. Framework for seismic performance assessment

3.1. Fragility function

The development of fragility curves of ACCRDs under short - and long - duration GMs are significant steps for seismic performance assessment according to the performance-based earthquake engineering (PBEE) framework. For the purpose of assessing the seismic performance of high dams, there have been several in-depth approaches to collecting the results for generating fragility curves, such as incremental dynamic analysis (IDA) (Vamvatsikos and Cornell, 2004), multiple stripe analysis (MSA) (Baker, 2015), and cloud analysis (Celik and Ellingwood, 2010). IDA is an efficient performance evaluation methodology, which linearly scaled from a low seismic intensity level to an extremely high seismic intensity level for each selected GMs. MSA is conducted at a specified set of seismic intensity level, each of which has engineering demand parameters (EDP). As the type of results

177 collected in these two methods differs, the effectively approach for estimating fragility curves from
178 the results also differs. It is worth noting that the efficient fragility estimates of IDA may be lower than
179 MSA for a given number of high performance structures. In this study, the fragility curves for the
180 ACCRD are investigated employing the MSA approach. Besides, the PGA of GMs is acknowledged
181 as the variable on behalf of the intensity measure (IM) of short - and long – duration GMs, and is
182 scaled from 0.1g to 0.7g in gaps of 0.1g.

183 As a critical and integrated component of a PBEE framework (Fajfar, 2000), the mainly purpose
184 of FR is to quantify the probability of exceedance (POE) relationships between structural damage state
185 with the various IM level. The fragility curves of an ACCRD can be conducted by a lognormal
186 cumulative distribution function (Baker, 2015):

187 $$FR(x) = \Phi\left(\frac{In(x/\theta)}{\beta}\right) \tag{4}$$

188 where $FR(x)$ is the POE that the structural damage state under a particularly seismic intensity level
189 reaching the specific DS; θ and β are the median and the logarithmic standard deviation of the
190 fragility function (the seismic intensity level with 50% POE) that is connected with the EDP and
191 structural capacity (Baker, 2015), respectively; Φ is the fragility curves function that belong to the
192 normal cumulative distribution. It is worth noting that the generally lognormal distribution is not only
193 one methodology that can be applied on Eq. (4). In this study, the methodology of MSA and maximum
194 likelihood estimate (MLE) is employed to fit the fragility curves.

195 On the basis of MSA-MLE, an analytical estimation approach is depicted in the present study to
196 generate the FR. At different seismic intensity level $IM = x_i$, the time – history analyses conduct
197 some number of collapses out of N_i total number of Nevertheless, early several study methodologies

198 on the sensitive extent of seismic behavior of structures under different GMD are obviously mixed
199 results. GMs. Assuming that collection of EDPs from short - and long - duration GMs are
200 independent of collections from other GMs, the probability of observing n_i collapses out of n_j
201 GMs with $IM = x_j$ is given by the binomial distribution:

202 $$P\left(n_i \text{ collapses in } N_i \text{ short and long ground motions} \middle| IM = IM_i\right) = \binom{N_i}{n_i} p_i^{n_i} \left(1 - p_j\right)^{N_i - n_i} \quad (5)$$

203 where p_i is the probability of collapse of the structure under short - and long – duration GMs with
204 $IM = IM_i$.

205 Following the MLE approach, the way to identify the fragility function for p_i is to select the
206 function that gives us the highest probability of observing the collapse data that was originated from
207 nonlinear dynamic analysis. Subsequently, the product of binominal probabilities according to Eq. (5)
208 at each IM levels, is employed to get the likelihood in the entire database.

209 $$Likelihood = \prod_{i=1}^{m} P\left(n_i \text{ collapses in } N_i \text{ short and long ground motions} \middle| IM = IM_i\right) = \prod_{i=1}^{m} \binom{N_i}{n_i} p_i^{n_i} \left(1 - p_i\right)^{N_i - n_i}$$

210 (6)

211 where m is the number of short - and long - duration GMs at each IM levels; $\prod$ represent a
212 product over all dates.

213 To conduct this maximize the likelihood function, p_i is replaced by the Eq. (4), and estimation
214 of the key parameters $\hat{\theta}$ and $\hat{\beta}$ (logarithmic mean and standard deviation) are then obtained by this
215 likelihood function. It is worth noting that the estimation of parameters by maximizing the logarithm
216 of the likelihood, which is equivalent and numerically more efficient and easier than the maximizing
217 the likelihood function itself, so that the fragility function can be explicit as follows:

$$\hat{\theta},\hat{\beta}=\arg\max_{\theta,\beta}\sum_{i=1}^{m}\left[\ln\binom{N_i}{n_i}n_i\ln\left(\Phi\left(\frac{\ln(x_i)-\theta}{\beta}\right)\right)+(N_i-n_i)\ln\left(1-\Phi\left(\frac{\ln(x_i)-\theta}{\beta}\right)\right)\right] \quad (7)$$

Standard commercial software packages such as Matlab, R, python, or Microsoft Excel can be utilized to calculate the Eq. (7), and detailed code can be found in the work of Baker (Baker, 2015).

3.2. Definitions of seismic performance indicators

After the earthquake disaster, the potential failure mode (PFM) of high dams is generally depicted as a function of concrete stiffness degradation, concrete strength degradation, dam crest settlement, landslide, cracks and liquidation among others. Due to the complex combination of these PFMs, the unsatisfactory performance and uncontrolled failure mode of high dams can be regarded as a chain of events. In addition, high ACCRDs are the complex system mainly composed of rockfill, transition and asphalt concrete core, as shown in Fig. 6. Therefore, from the perspective of safe operation of complex hydraulic engineering, the employ of a single damage index to evaluate performance level of high ACCRDs may not be accurate enough and overestimate its ability to resist earthquakes. In this study, two damage indicators from different aspects have been applied to evaluated seismic performance of high ACCRDs under shorter duration and longer duration GMs.

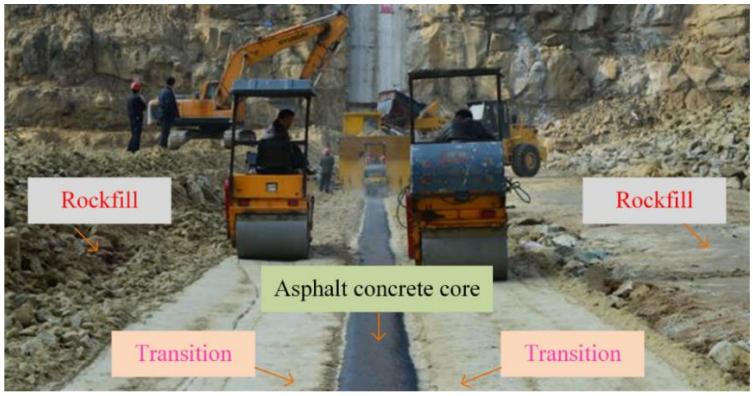

Fig. 6. Construction of high ACCRD.

The relative settlement ratio (RSR) of dam crest is one of the most generally seismic damage

modes of embankment dams. Swaisgood (2003) surveyed 69 embankment dams settlement and deformation, including concrete faced rockfill dams, earth core rockfill dams, earthfill dams, hydraulic fill dams, and recommended RSR of dam crest as an seismic performance index. Besides, the seismic performance index is divided the PFM situation into four performance levels: none ($<0.1\%$), minor ($0.012-0.5\%$), moderate ($0.1-1.0\%$) and severe ($>1\%$), as displayed in Fig. 7. Based on the work of Swaisgood et al. (2003), Wang et al. (2015) proposed the RSR of 0.1%, 0.4% and 1% as the assessment performance levels when this embankment dams reached to minor, moderate and severe. To more safely assess the seismic performance of the high ACCRD, the four performance levels of embankment dam proposed by Wang et al. (2015) is utilized in this paper.

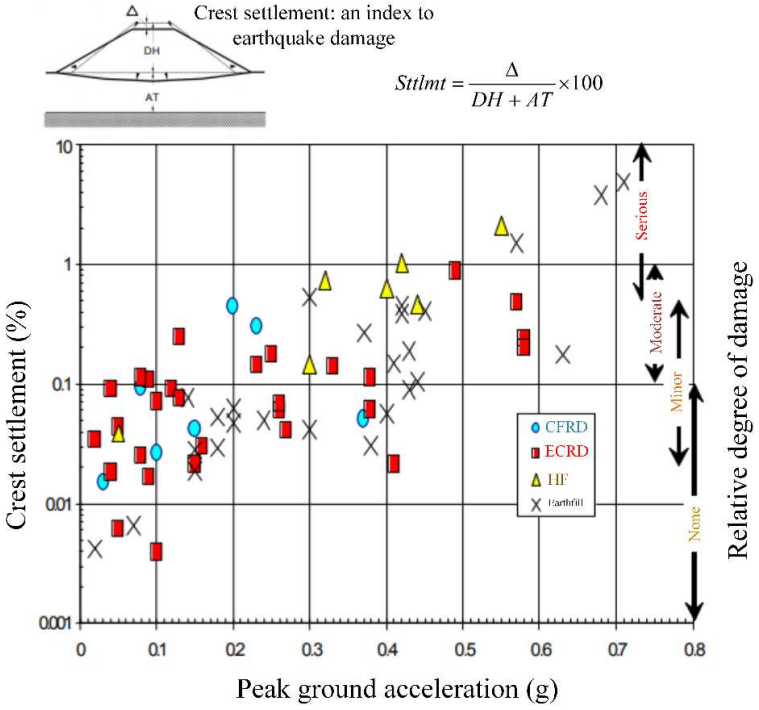

Fig. 7. Construction of high ACCRD.

The seismic performance of the asphalt concrete core, employed as an indispensable component of the impervious system, is one of major concerns in high ACCRD design. To account for the impacts of cyclic earthquake loading, a qualitative methodology assessed the seismic performance of concrete

249 materials structure is firstly proposed by Ghanaat (2004). Subsequently, the performance index is
250 widely employed to forecast the seismic performance of concrete gravity dams (Wang et al., 2014),
251 concrete arch dams (Ardebili and Mirzabozorg, 2012) and concrete face rockfill dams (Xu et al., 2020).
252 As shown in Fig. 8, the performance index is systematic and rational formulated in light of the stress
253 demand-capacity ratios (DCR), the cumulative inelastic duration (CID), overstressed regions of
254 concrete materials, and other considerations form the basis for an approximate and qualitative estimate
255 of damage. The DCR can be calculated according to the follow formula:

256 $$DCR = \frac{\sigma_d}{f_t} \tag{8}$$

257 where σ_d is the maximum tensile stress during dynamic analysis; f_t is ultimate tensile stress
258 strength of concrete materials.

259 The static tensile strength of concrete materials characterized by the standard un-axial splitting
260 tension experimental tests or from:

261 $$f_t = 1.7 f_c^{'2/3} \tag{9}$$

262 where f_c represent the static ultimate compressive strength of concrete materials. The maximum
263 permitted DCR of dams is 2 during the dynamic analysis, which means the maximum tensile stress
264 twice the ultimate tensile stress strength of the concrete materials. In this study, the experimental
265 compressive strength of the asphalt concrete is approximately 1.6 MPa under 10^{o} condition (Feng et
266 al., 2020; Ning et al., 2020, 2019), and the corresponding tensile strength of asphalt concrete can be
267 obtained from the Eq. (9).

268 The CID refers to the total duration of cyclic stress above a certain stress strength, which is related
269 to different DCR levels. As shown in Fig. 8(a), the hypothetical harmonic stress time - history

(oscillation period of 0.24s) includes 5 cyclic tensile stress (shaded area) exceeding the specific tensile strength. Between one oscillation period, the CID of the stress excursion beyond the upper tensile strength (shaded area) is taken equal to 0.8s ($T/3$). The total cumulative inelastic duration ($DCR \geq 1$) for all 5 cycles exceeding the tensile strength amounts to 0.4s. Moreover, it can also be found from Fig. 8(a) that the CID for a $DCR = 2$ is assumed 0. Based on the high dams resist loads mechanism, the cumulative duration of 0.3s, 0.4s and 0.6s is respectively for gravity dams (Wang et al., 2014), arch dams (Ardebili and Mirzabozorg, 2012) and concrete face rockfill dams (Pang et al., 2018; Xu et al., 2020). In view of the fact that the recovery capacity of asphalt concrete and the resist loads mechanism of asphalt concrete core is similar to gravity dams (cantilever mechanism), the CID is taken as 0.35 in this paper. On the hand, the seismic performance of high ACCRDs is evaluated on the basis of the combined criteria and their possible coupling (DCR-CID). Three performance levels are considered according to the aforementioned assessment methodology:

1. Minor or no damage. The tensile stress of asphalt concrete core response is lower than extremely tensile strength of asphalt concrete, which means the asphalt concrete core is in a no or minor damage if $DCR \leq 1$.

2. Moderate damage. The asphalt concrete core will exhibit inelastic behavior in the form of damage cracking if the estimated $DCR > 1$. If the estimated $1 < DCR < 2$, $0 < CID \leq 3.5$ for all DCR's, and overstressed regions are less than 15% of the asphalt concrete core, it is considered that the asphalt concrete core is acceptable with no possibility of failure, as shown in Fig. 9

3. Severe Damage. The damage state of the asphalt concrete core is regarded as severe when $DCR > 2$, or $3.5 < CID$ for all DCR's given in Fig. 9.

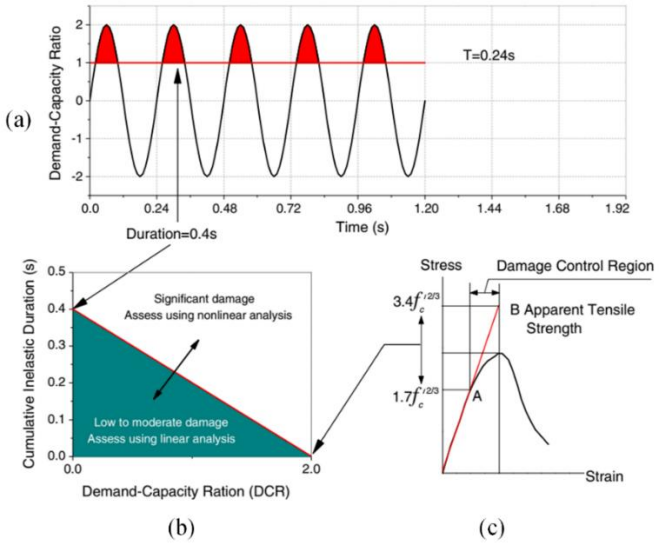

291

292 **Fig. 8.** Illustration of seismic performance and damage criteria (Ghanaat, 2004).

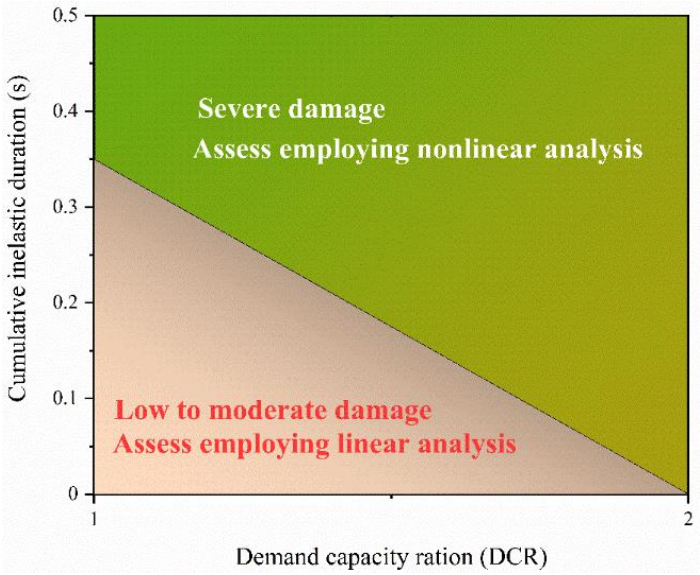

293

294 **Fig. 9.** Seismic performance and limit state threshold value of asphalt concrete core.

295 ## 4. Numerical case study

296 ### 4.1. Engineering background of the Dashimen dam

297 Dashimen dam is located on the Cheerchen River in Bayingol mongolian autonomous prefecture

298 (Xinjiang, China) and started construction in January 2018. It is planned to achieve the goal of

impounding water for Dashimen dam in October 2020. Dashimen dam is currently the highest asphalt concrete core rockfill dam in Xinjiang, with a maximum crest height of 130 m, a crest length of 205 m, and a crest width of 12 m (see Fig. 10). The asphalt concrete core adopts the geometric form of upper narrow and lower width. As shown on the Fig. 10, the top width and the bottom width of asphalt concrete core is 0.6 m and 1.4 m, respectively. In addition, there is a magnifying foot with a height of 3.2 m, and the thickness of the magnifying foot changes gradually from 1.4 m to 2.6 m. The total storage capacity of the reservoir is 127 million cubic meters, and the adjusted storage capacity is 99 million cubic meters. The bedrock materials are composed of diabase, Jurassic mudstone, sandstone and sand pebble bed. On the other hand, Dashimen dam is located in the regions where strong earthquakes frequently occur with design peak ground acceleration (PGA), $PGA=0.52g$. Seismic performance of Dashimen dam under different seismic intensities GMs is a crucial factor for the hydraulic engineering.

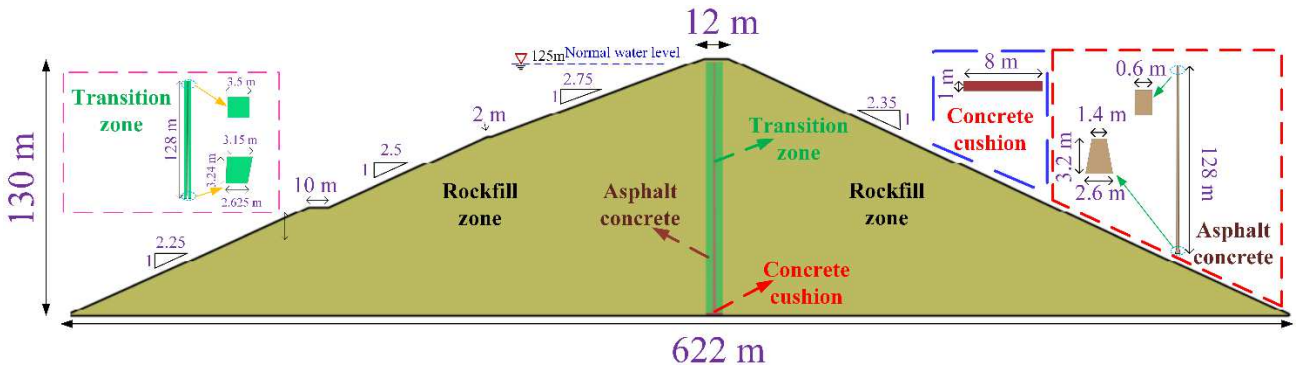

Fig. 10. Construction and design of Dashimen dam: (a) aerial view; (b) cross section

4.2. Finite element model considering the dam – water – foundation interaction system

The FE model is developed utilizing in the commercial software ABAQUS. The FE model of dam – reservoir – foundation (DRF) interaction system is discretized into an assemblage of solid

element, as decipted in Fig. 11. In these models, rockfill zone, transition zone, asphalt concrete core, concrete cushion, foundation rock and reservoir water have 41742, 4032, 1344, 108, 132840 and 51318 finite elements, respectively. Moreover, 672 interface elements were defined in asphalt concrete core – transition zone interface. The total numbers of integration points of the Dashimen dam body, foundation rock and reservoir water are 57232, 157990 and 61138, respectively. To more precisely simulate the seismic behaviour of the asphalt concrete core, four layers of spatial 8-node isoparametric elements is employed to model the core thickness.

Before the time-history dynamic analyses, the initial stress condition for Dashimen dam needs to be determined by static analysis. As shown in Fig. 11, the Dashimen dam reproducing a staged construction and staged water impounding are step – by – step and are modelled with 11 steps and 12 steps, respectively. To reflect the extremely unfavorable water table of Dashimen dam, the presence of water in the reservoir is assumed the case of full reservoir, which is impounded from dam base to dam crest after dam construction was completed. Moreover, the water pressure is applied on the upstream face of asphalt concrete core and concrete cushion by means of a triangular hydrostatic profile. The static boundary conditions are restrained in the x, y and z directions at the bottom truncated boundary. For left and right boundaries, the static boundary conditions are fixed only in the lateral direction and are free in the y direction. On the other hand, the front and back static boundary conditions of dam and foundation rock are restrained in the z direction. During the filling and impounding process, the typical hyperbolic Duncan Chang E-B model (Duncan and Chang, 1970) is used to describe the pre-seismic stress–strain for rockfill zone, transition zone and asphalt concrete core. The detailed material parameters of the Duncan E-B model are described in Table 3.

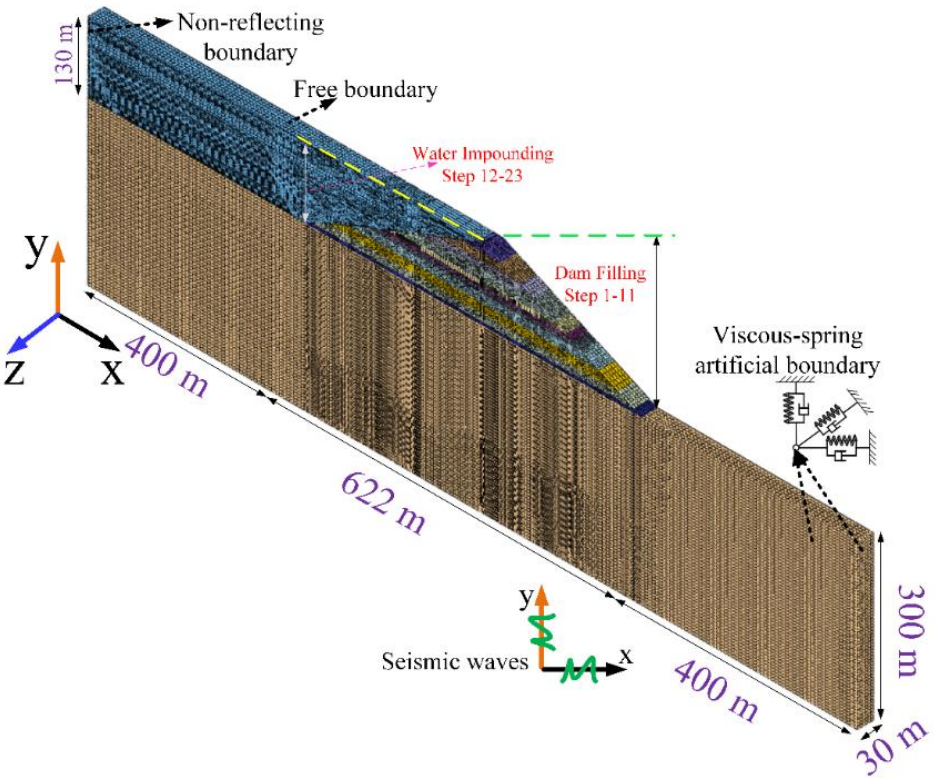

(a)

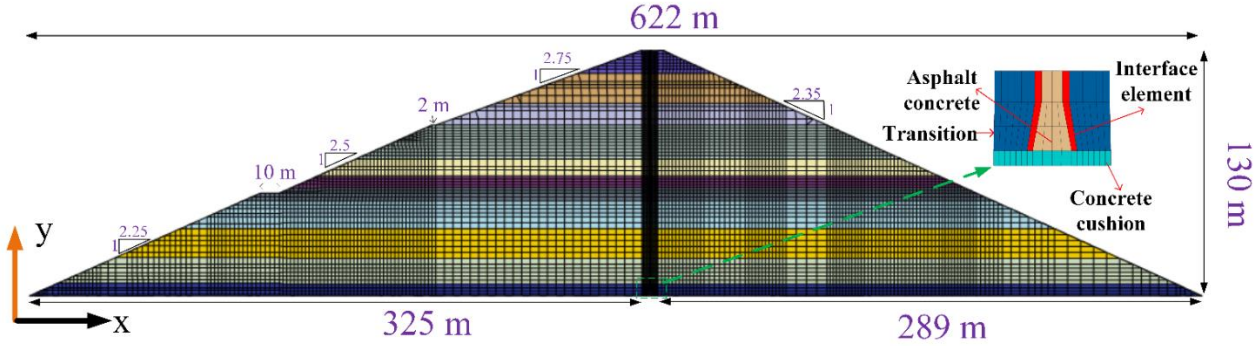

(b)

Fig. 11. Details of the high ACCRD – water – foundation FE model.

Table 3 Material parameters for Duncan E-B model (Kong et al., 2014; Li et al., 2020)

Materials	$\rho/(\mathrm{kg/m^3})$	K	n	R_f	K_b	m	$\varphi_0/(\mathrm{o})$	$\Delta\varphi_0/(\mathrm{o})$
Rockfill	2150	750	0.6	0.78	450	0.05	36	7.5
Transion	2200	1000	0.55	0.8	700	0.1	42	6.5
Asphalt concrete	2420	429.1	0.603	0.88	944	0.495	25.4	0

In dynamic analyses of embankment dam, the equivalent linear viscoelasticity model (Hardin and

Drnevich, 1972) have been widely used in practical engineering to reflect the mechanical seismic behavior of rockfill zone, transition zone and asphalt concrete core (10^{o}). Moreover, the model of parameters are easily obtained from the experiment test. According to Hardin and Drnevich's postulation which indicates that the maximum dynamic shear modulus of a damming rockfill and asphalt concrete is formulated as follows (Hardin and Drnevich, 1972):

$$G_{\max} = K \cdot p_a \cdot \left(p / p_a \right)^n \tag{10}$$

where K and n is the experimental parameters, respectively; p_a represent the standard atmospheric pressure; p is the average effective stress. The detailed model parameters are listed in Table 4.

Table 4 Parameters for Hardin - Drnevich model (Kong et al., 2014; Li et al., 2020)

Materials	K	n	v
Rockfill	2270	0.273	0.22
Transion	2700	0.375	0.22
Asphalt concrete (10^{o})	1979	0.4	0.345

The cycle earthquake load will induce the high ACCRDs to generate irrevocably permanent deformation. However, the equivalent linear viscoelasticity model is only used to obtain the time history curves of the shear strain, stress and acceleration, whereas the methodology cannot directly obtain the permanent deformation of the dam body. Currently, there are many acceptably numerical models according to the equivalent nodal force approach that are utilized to compute the permanent deformation, such as the Serff and Seed model, the IWHR model, Taniguchi model, improved Taniguchi model, Shen Zhu-jiang model and improved Shen Zhu-jiang model. The permanent deformation of dam body is calculated according the work of Serff and Seed model (Serff et al., 1976). Moreover, the relationships based on dynamic triaxial experiments and Shen Zhu-jiang model (Zhu-

Jiang and Gang, 1996) of drainage conditions among the residual dynamic volumetric strain increment $\Delta\varepsilon_{vr}$, the residual dynamic shear strain increment $\Delta\gamma_r$, the dynamic stress state and the vibration duration can be expressed as follows (Zhu-Jiang and Gang, 1996):

$$\Delta\varepsilon_{vr} = c_1\gamma_d^{c_2}\exp\left(-c_3 S_1^2\right)\frac{\Delta N}{1+N} \tag{10}$$

$$\Delta\gamma_r = c_4\gamma_c^{c_5} S_1^n \frac{\Delta N}{1+N} \tag{11}$$

where c_1, c_2, c_3, c_4,and c_5 are the experimental test parameters; γ_d represents the dynamic strain amplitude; ΔN and N is the time increment and total vibration times, respectively; S_1^n is the stress level; n is the stress level index and is generally $0.9-1.0$.The detailed permanent deformation model parameters of the rockfill materials are shown in Table 5.

Table 5 Parameters for permanent deformation (Li et al., 2020)

Materials	$c_1/(\%)$	c_2	c_3	$c_4/(\%)$	c_5
Rockfill	0.72	0.96	0	9.34	0.37
Transion	0.56	0.42	0	8.25	0.4

For the concrete cushion, the mechanical responses and dynamic cracking mechanism is specifically described by the concrete damage plastic (CDP) model in the ABAQUS material library. The CDP model is firstly proposed by Lubliner et al. (1989) and improved by Lee and Fenves (1998). Many previous studies demonstrate that the CDP model can particularly for simulating the realistic dynamic crack profiles in concrete materials (Huang et al., 2017; B. Sun et al., 2020; Benbo Sun et al., 2020b; Wang et al., 2019). The foundation rock of Dashimen dam is assumed to be linearly elastic model. Table 6 present the detailed material parameters of foundation rock and concrete cushion.

Table 6 Material parameters of bedrock and concrete cushion.

Material	Constitutive model	Input parameter	Value
(a) foundation rock	Linear elastic	Mass density	2730

		P (kg/m^3)	
		Elastic modulus (GPa)	5.0
		Poisson's ratio	0.25
(b) Concrete cushion	Concrete damage plastic model	Mass density ρ (kg/m^3)	2450
		Elastic modulus (GPa)	28
		Poisson's ratio	0.167
		Tensile yield stress (MPa)	1.78
		Compressive yield stress (MPa)	16.7
		Dynamic magnification factor	1.2

Generally, to obtain more accurate numerical results, the contact element should be defined to reflecting the interface behavior between two materials with significantly different mechanical property. In this paper, the Goodman zero-thickness contact element is used to simulate the transition – concrete interface. Moreover, the thin-layer contact element (5 cm) is applied between transition and asphalt concrete to revel the contact behavior. Although many models have been proposed to reflect the strain – stress relationship of contact element, a Clough – Duncan hyperbolic model is employed for the contact element and the parameters of hyperbolic model can be easily obtained from shear test experiment. The dynamic hyperbolic model developed by Wu et al. (1992) is applied to simulate the dynamic behavior of the contact element. The detailed parameters of the contact element are presented in Tables 7 and 8.

Table 7 Parameters for static contact element (Ji, 2006)

Contact element	Materials	K	n	φ	R_f
Thin-layer contact element	Transition – asphalt concrete	3200	0.42	27	0.65
Goodman zero-thickness contact element	Transition-concrete cushion	5600	0.52	36	0.86

Table 8 Parameters for dynamic contact element (Ji et al., 1995; Wu et al., 1992)

Contact element	Materials	C	M	δ	λmax
Thin-layer contact element	Transition – asphalt concrete	300	0.96	0.58	0.15
Goodman zero-thickness contact element	Transition-concrete cushion	22	2.0	34	0.2

For embankment dams, hydrodynamic pressure generally has no significantly effect on the dam

394 crest accelerations (Pelecanos et al., 2016). However, the stress and strain of the upstream dam body
395 may be sensitive to hydrodynamic pressure (Pelecanos et al., 2020). To simulate the DRF dynamic
396 interaction system, fluid elements, which represent a linearly elastic inviscid, irrotational, and
397 compressible medium, are used to model the reservoir. In addition, the coupled Lagrangiann
398 formulation of FE method is directly conduct for seismic dynamic analysis of interacting DRF systems.
399 As illustrated in Fig. 11(a), the upstream face of the reservoir is set as non-reflecting boundary
400 condition to enable energy dissipation during the dynamic analysis process. The direction normal
401 displacement is assumed to simulate the interface between the reservoir and the dam following the
402 recommendations of Wang et al. (2018). At the dam – foundation interface, the reservoir is tied with
403 the foundation of the dam. The material mechanical properties of the fluid element can be found in our
404 previous work of Wang et al. (2015). The typical damping ratio for DRF dynamic interaction system
405 is assumed as 5% in time - history dynamic analyses. Rayleigh damping, calculated by two parameters
406 obtained from modal damping ratios of the DRF dynamic interaction system, is considered in time-
407 history dynamic analyses.

408 **4.3. Seismic wave input mechanism**

409 An effective and reasonable GM input mechanism is required to ensure the stability and accuracy
410 of the numerical results before the dynamic analysis of Dashimen dam. Recently, the methodology in
411 which the near-field numerical calculation region is extracted from a semi-infinite elastic medium is
412 commonly applied on the hydraulic engineering. Liu et al. (2006) proposed widely employed viscous-
413 spring artificial boundary (VASB) with good high-frequency and low-frequency stability. Moreover,

414 the VSAB can absorb scattered waves and reflect the elastic recovery feature of a semi-infinite medium
415 under strong GM excitation. The VSAB is generally employed on the truncated boundary of
416 foundation, as display on Fig. 11(a). On the other hand, the horizontal and vertical component of GM
417 excitation can be simulated by converting the time – history of GM into time – history of equivalent
418 nodal forces of truncated boundary nodes according to the work of Liu et al. (2006). The equivalent
419 nodal force f_{li} of truncated boundary nodes l in direction can be derived as follows:

420 $$f_{li} = K_{li} d_{li}^{f} + C_{li} v_{li}^{f} + \sigma_{li}^{f} \tag{12}$$

421 where K_{li} and C_{li} represents the parameter of stiffness and damping coefficients for spring – damper;
422 d_{li}^{f}, v_{li}^{f} and σ_{li}^{f} represent displacement vector, velocity vector, stress vector at the truncated
423 boundary node l, respectively (Du and Zhao, 2006). The detailed seismic wave input method and
424 validation cases in the infinite elastic medium can be found in our previous work (Benbo Sun et al.,
425 2020b, 2020c, 2020a).

426 **5. Fragility analysis and discussion**

427 **5.1 Relative settlement ratio index**

428 Results of the dynamic analyses show that the ID of strong GMs take a significant effect on the
429 RSR of a high ACCRD, as shown in Fig. 12. This figure shows the RSR of a high ACCRD under long
430 - duration is mostly greater than that under short - duration. To interrogate the differences in the RSR
431 of a high ACCRD under shorter duration and longer duration GMs, the mean value of the RSR under
432 different seismic intensities is compared in Fig. 13. As displayed in Fig. 13, the difference between
433 short - duration GMs and long - duration GMs increases as the seismic intensity increases. This

observation means that the coupling of high intensity GMs and long - duration may induce serious damage for a high ACCRD.

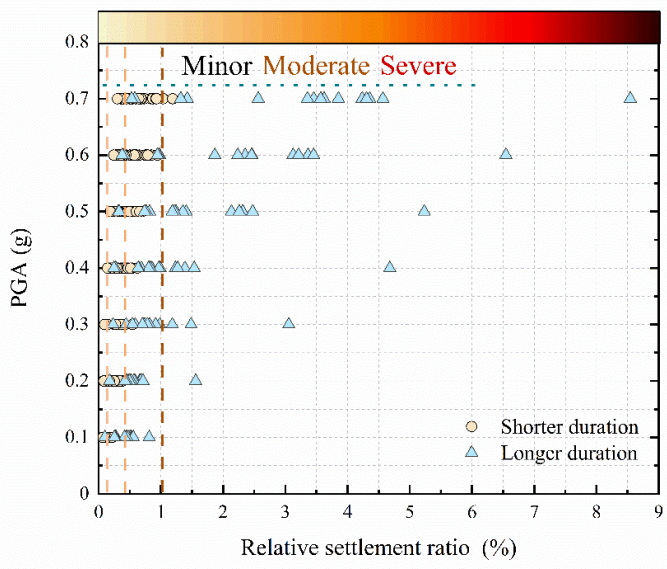

Fig. 12. The RSR of multiple strip response under different seismic intensities.

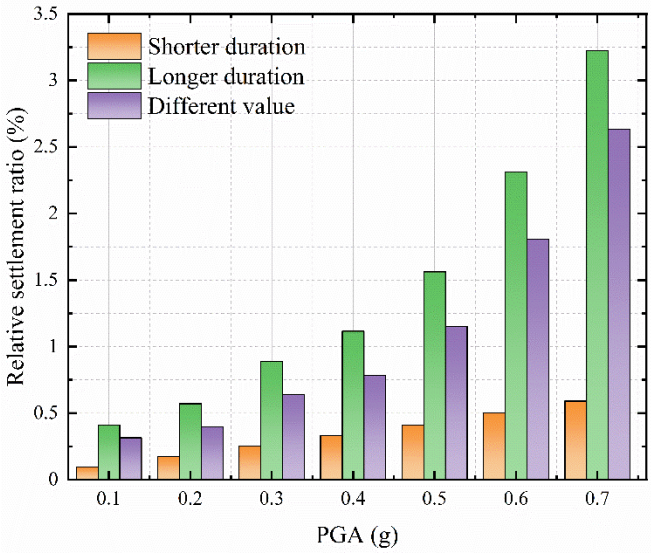

Fig. 13. Mean value of RSR.

The seismic fragility curves for the minor, moderate and severe performance levels obtained from Eq. (7) are given in Fig. 14. For simplicity of illustration, this figure provides presents the comparison of seismic fragility curves of short - and long - duration GMs for different performance levels. For the same performance levels, the seismic fragility curve for the short - duration is uniformly situated to

444 the right of the seismic fragility curve of long - duration, meaning the increasing POE when the high
445 ACCRD is excited by long - duration GMs. Currently, the seismic design of high dams generally
446 consider two seismic levels to assure structural safety, containing the operating basis earthquake (OBE)
447 and the maximum credible earthquake (MCE). For this high ACCRD, the OBE and MCE stipulated in
448 the actual engineering project situation is defined as 0.4g PGA and 0.54g PGA, respectively. Figure
449 15 further list the POE of RSR in different performance level. The highest POE is given by long -
450 duration GMs of the order of 100% in Minor damage, 95% in moderate damage, 54% in severe damage
451 under MCE excitation.

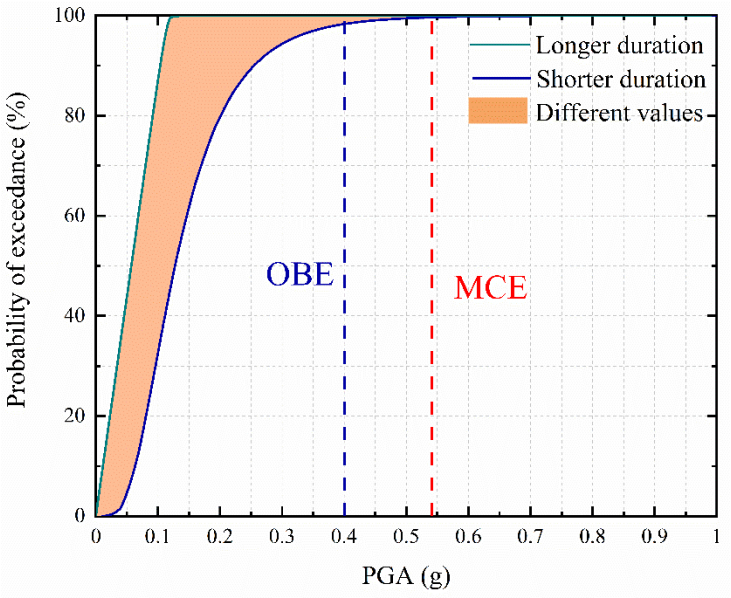

452

453 (a) Minor

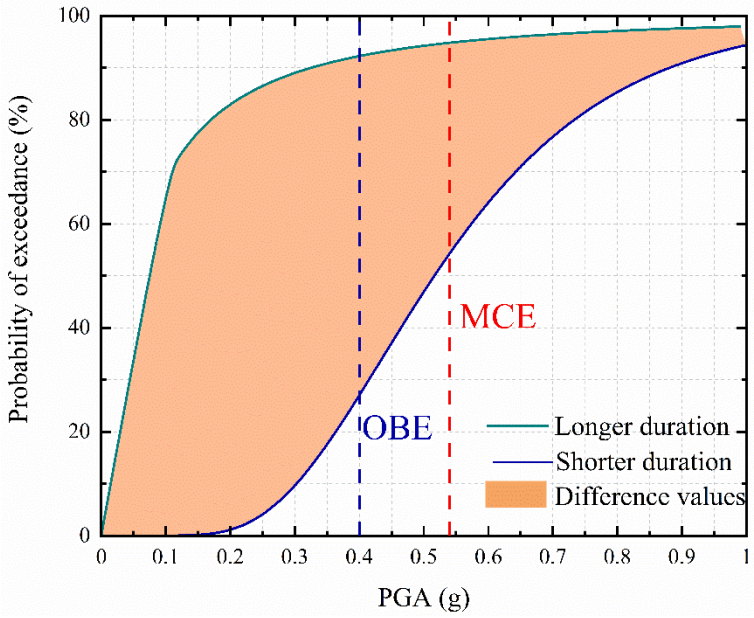

(b) Moderate

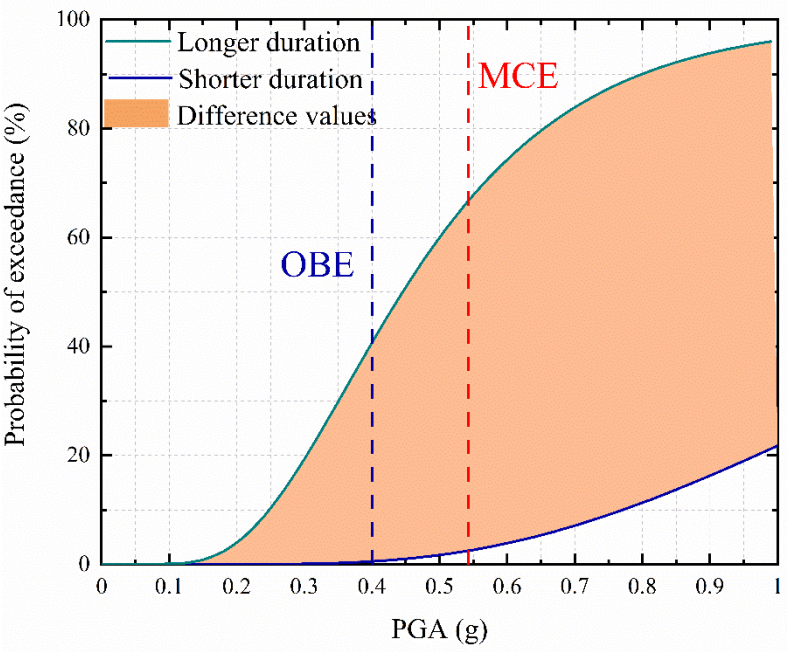

(c) Severe

Fig. 14. Comparison of fragility curves of short - and long - duration GMs for different performance levels: (a) Minor damage. (b) Moderate damage, and (c) Severe damage.

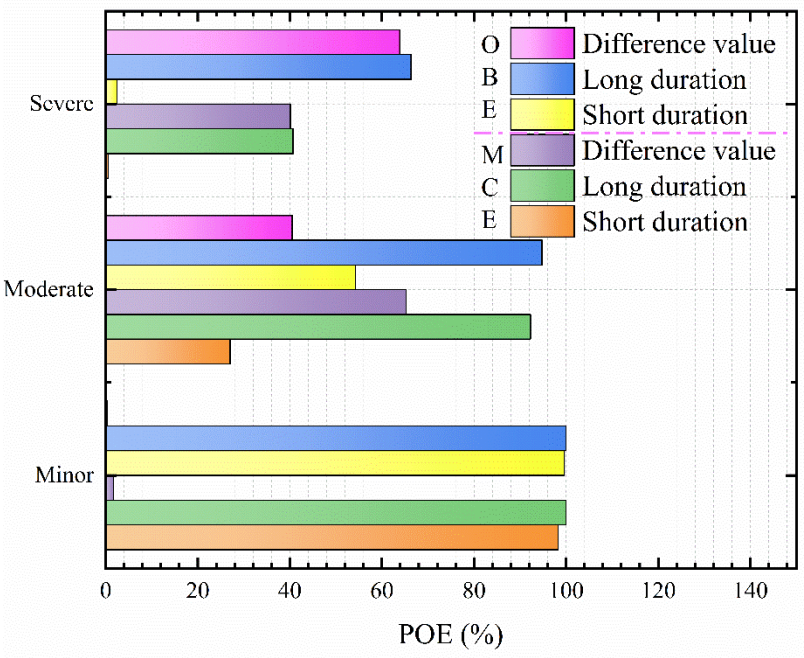

460

461 **Fig. 15.** The POE of different performance levels of RSR under OBE and MCE.

462 **5.2 The stress demand-capacity ratios and cumulative inelastic duration index**

463 The seismic performance evaluation based on the DCR-CID is utilized to assess the performance
464 levels of the ACCRD subjected to short - and long - duration GMs. Figures 16(a) presents the
465 maximum principle tensile stress time histories for short - and long - duration GMs with a PGA level
466 of 0.5g. The corresponding performance evaluation curves are illustrated in Fig. 16(b). It is clear from
467 Fig. 16(a) that the long - duration records make the number of cycles that excess of the tensile strength
468 of the asphalt concrete greater than the short - duration. Results in Fig, 16(b) display that the stress
469 DCR exceed 1 or 2 and the CID under long - duration GMs are significantly greater than the short -
470 duration. In addition, the DCR-CID under short - duration GMs with a PGA level of 0.5g are in the
471 range of low to moderate damage. The DCR-CID seismic fragility curves obtained at each damage
472 levels for the asphalt concrete core is shown in Fig. 17. It is evident from this figure that the effect of

GMD on the seismic fragility curve of the high ACCRD is maximal for the two damage levels, while a significantly difference value of POE can be found. Overall, the probability of exceeding the each performance levels under long - duration is greater that the POE under short - duration. Furthermore, the probability of exceeding the severe performance level under strong GMs is below the 50%, which means the asphalt concrete core can perform its engineering function under extremely earthquake excitation. For simplicity of illustrate the difference characteristic of short - duration and long - duration, Fig. 18 list the POE of two performance levels of DCR-CID under OBE and MCE. Comparing short - duration and long - duration under OBE and MCE in Fig. 18 shows that they are generally different from each other. For instance, the difference value between short - duration and long - duration for POE of moderate damage is 20.2% at OBE, 20.8% at MCE, corresponding the POE of severe damage is 9.2% at OBE, 12.8% at MCE.

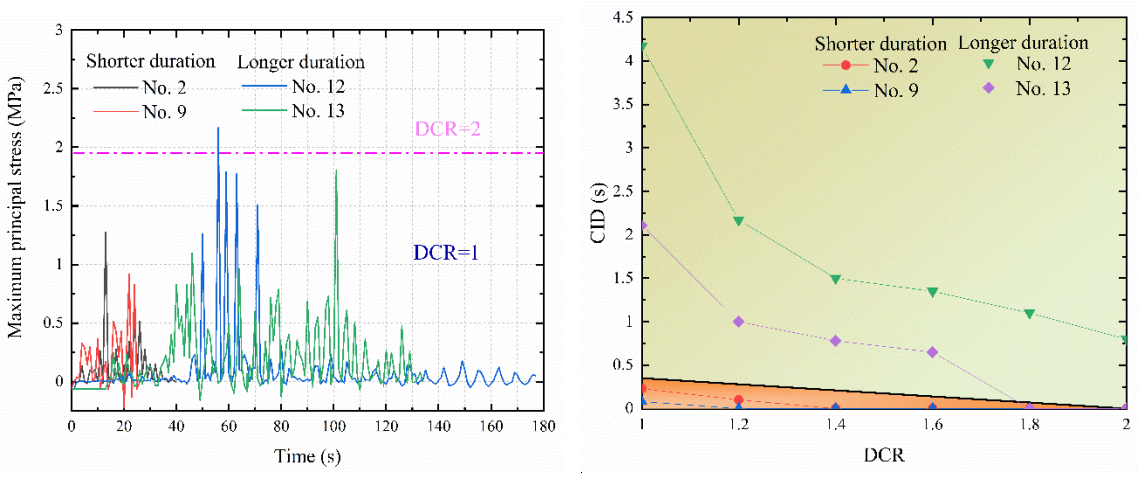

(a) Time histories of maximum principal stress (b) Performance assessment curves

Fig. 16. Time histories of maximum principal stress and performance assessment curves for short - and long - duration GMs with a PGA level of 0.5g.

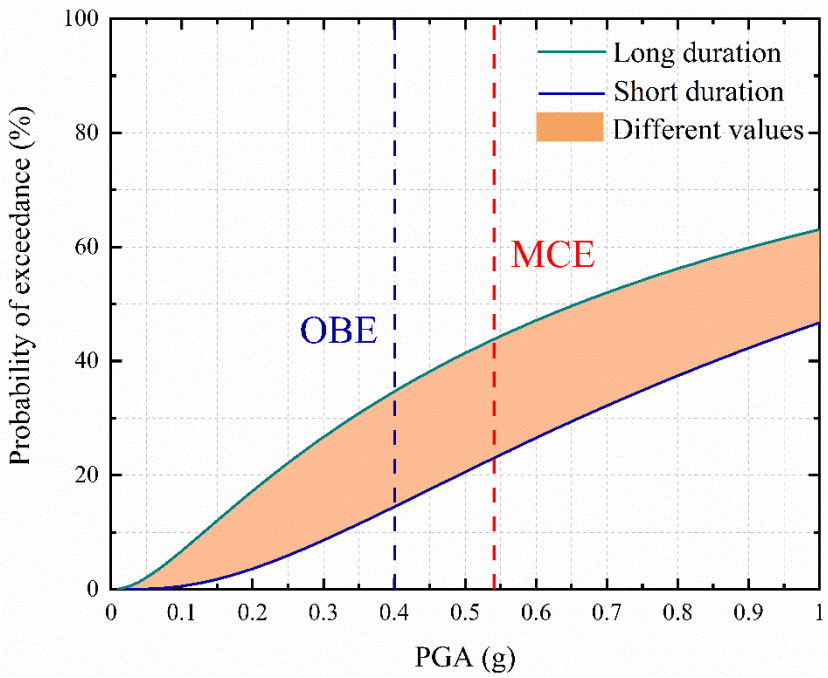

(a) Moderate

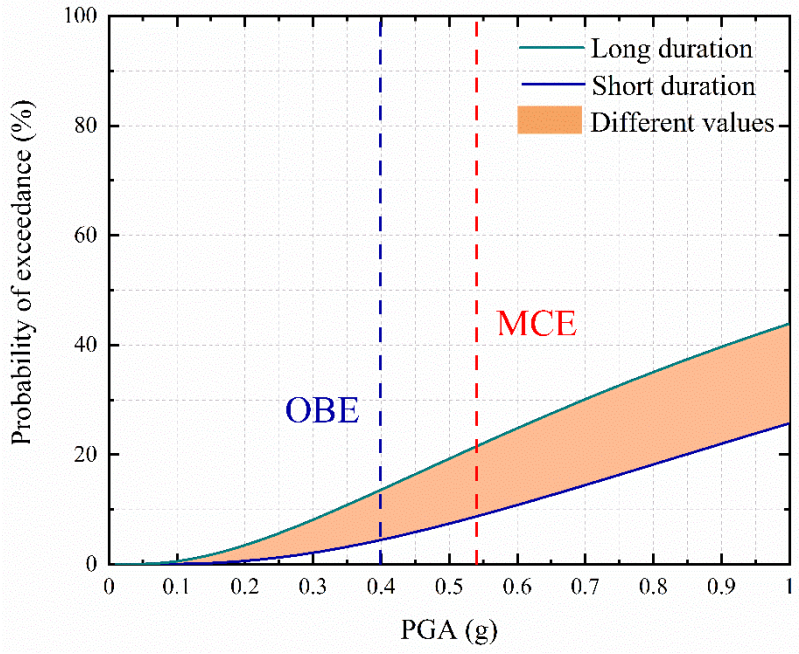

(b) Severe

Fig. 17. Seismic fragility curves with short - and long - duration GMs for (a) moderate; (b) severe.

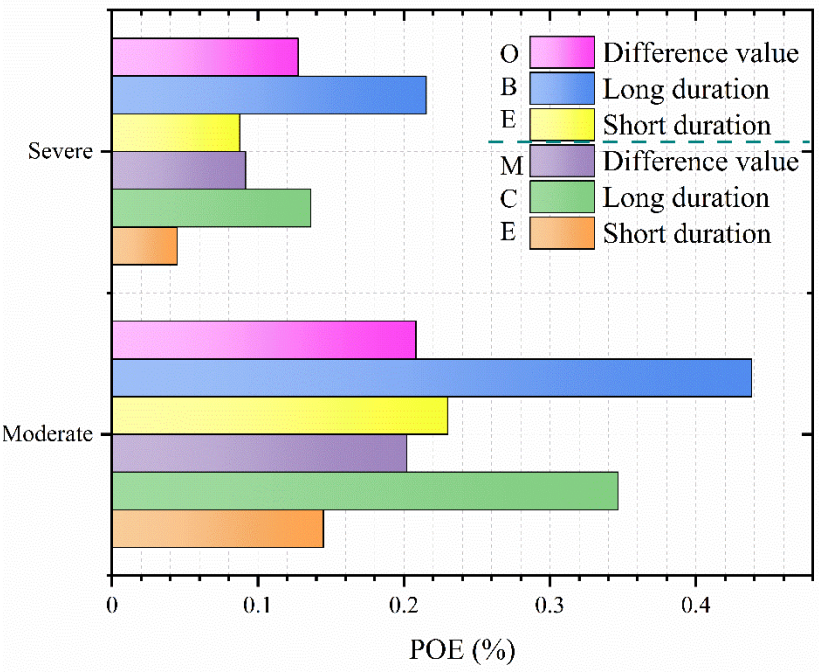

Fig. 18. The POE of different performance levels of RSR under OBE and MCE.

6. Summary and conclusions

This study entirely studied the impact of short - and long - integrated duration (ID) on the seismic fragility analysis (FR) of a high asphalt concrete core rockfill dam (ACCRD) considering dam – reservoir – foundation (DRF) dynamic interaction system. A series of seismic dynamic analysis of finite element model were conducted to generate 322 numerical results to determine the seismic fragility curves of a high ACCRD via coupling multiple stripe analysis and maximum likelihood estimate.

In this particular study, the developed multiple stripe data showed that the relative settlement ratio (RSR) of a high ACCRD is more vulnerable to moderate damage or severe damage when subjected to longer duration. Furthermore, the results of the system fragility curves indicate that for damage states for which the high ACCRD behaves under strong GMs, there is significantly effect due to the different

ID on the fragility curves and risk. The damage state of a high ACCRD under shorter duration exhibit smaller seismic fragilities. Such phenomenon is explained by the fact that for the the operating basis earthquake (OBE) or the maximum credible earthquake (MCE), the longer duration may trigger severe damage of a high ACCRD.

The impact of ID on the stress DCR and CID demonstrates that the stress DCR exhibits sensitivity to the longer duration, while the CID also shows relatively strong sensitivity to the longer duration. It is reasonable that the longer duration, the greater DCR-CID, since the performance index is related to the duration of cycles exceeding the tensile strength of the asphalt concrete core. Similarly, the developed seismic fragility curves for the asphalt concrete core under longer duration exhibited significantly higher POE than shorter duration. In addition, the difference value of POE between short - duration and long - duration is increase along with the increase seismic intensity. The study provides important insight into the seismic behavior of the high ACCRD and highlights the need for further development of seismic design codes in consideration of the impact of ground motion duration, frequency, amplitude.

Finally, several restrictions of the present study should be paid more attention. Among the effect of real environment, the dam-reservoir-foundation dynamic interaction system is more complex, so only the effect of hydrodynamic pressure is considered. Further, the tensile strength of asphalt concrete is approximately determined according the work of Ghanaat (2004). Further research should consider the shaking model test and numerical analysis with more than two performance indictors or with different elastic-plastic analysis combinations of the multi-field coupling approach.

Acknowledgments

The authors gratefully appreciate the support from the National Natural Science Foundation of China (No.51979188 & No.51779168), National Key Research and Development Program of China (No. 2018YFC0406901)

Declarations

Conflict of interest The authors declare no conflict of interest.

References

Ardebili, M. H. and Mirzabozorg H. (2012) Effects of near-fault ground motions in seismic performance evaluation of a symmetric arch dam. *Soil mechanics and foundation engineering*, 49(5), 192-199.

Baker, J. W. (2015) Efficient analytical fragility function fitting using dynamic structural analysis," *Earthquake Spectra*, 31(1), 579-599.

Barbosa, A. R., Ribeiro, F. L., and Neves, L. A. (2017) Influence of earthquake ground‐motion duration on damage estimation: application to steel moment resisting frames. *Earthquake Engineering & Structural Dynamics*, 46(1), 27-49.

Baziar, M. H., Salemi, S. H., and Merrifield, C. M. (2009) Dynamic centrifuge model tests on asphalt-concrete core dams. *Geotechnique*, 59(9), 763-771.

Bolt, B.A. (1973) Duration of strong ground motion. in: Proceedings of the 5th World Conference on Earthquake Engineering, pp. 1304–1313.

Bommer, J. J., and Martinez-Pereira, A. (1999) The effective duration of earthquake strong motion. *Journal of earthquake engineering,* 3(02), 127-172.

546 Bommer, J. J., Stafford, P. J., and Alarcón, J. E. (2009) Empirical equations for the prediction of the significant,
547 bracketed, and uniform duration of earthquake ground motion. *Bulletin of the Seismological Society of America*,
548 99(6), 3217-3233.
549 Celik, O. C., and Ellingwood, B. R. (2010) Seismic fragilities for non-ductile reinforced concrete frames–Role of
550 aleatoric and epistemic uncertainties. *Structural Safety*, 32(1), 1-12.
551 DU, X. L. and ZHAO, M. (2006) Analysis method for seismic response of arch dams in time domain based on
552 viscous-spring artificial boundary condition. *Journal of Hydraulic Engineering*, 9, 1063-1069. (in Chinese)
553 Duncan, J. M., and Chang, C. Y. (1970) Nonlinear analysis of stress and strain in soils. *Journal of Soil Mechanics &*
554 *Foundations Div*.
555 Fajfar, P. (2000) A nonlinear analysis method for performance‐based seismic design. E*arthquake spectra*, 16(3),
556 573-592.
557 Feng, S., Wang, W., Hu, K., and Höeg, K. (2020) Stress-strain-strength behavior of asphalt core in embankment dams
558 during construction. *Construction and Building Materials*, 259, 119706.
559 Ghanaat, Y. (2004) Failure modes approach to safety evaluation of dams. in: Proceedings of the 13th World
560 Conference on earthquake engineering.
561 Green, R. A., and Terri, G. A. (2005) Number of equivalent cycles concept for liquefaction evaluations—Revisited.
562 *Journal of Geotechnical and Geoenvironmental Engineering*, 131(4), 477-488.
563 Hardin, B. O., and Drnevich, V. P. (1972) Shear modulus and damping in soils: design equations and curves. *Journal*
564 *of Soil Mechanics and Foundations Div*, 98(sm7).
565 Huang, J. Q., Du, X. L., Zhao, M., and Zhao, X. (2017) Impact of incident angles of earthquake shear (S) waves on
566 3-D non-linear seismic responses of long lined tunnels. *Engineering Geology*, 222, 168-185.

567 Chunlou, J., Songyou, X., and Desheng, D. (1995) Dynamic Analysis of Asphalt Concrete Core Rockfill Dams on
568 Deep Overburden. *JOURNAL OF HOHAI UNIVERSITY (NATURAL SCIENCES)*, 5.
569 Ji, H. (2006) 3-D FEM Dynamic Analysis on Asphalt Concrete Core-wall Rockfill Dam Built on Deep Overburden
570 Layers." *Hohai University*.
571 Jun-shuai, W. U., and JIANG, P. (1992) Dynamic shearing characteristics of soil-concrete interface. *Chinese Journal*
572 *of Geotechnical Engineering*, 14(2), 61-66.
573 Kitayama, S., and Constantinou, M. C. (2020) Implications of strong earthquake ground motion duration on the
574 response and testing of seismic isolation systems. *Earthquake Engineering & Structural Dynamics*.
575 Kong, X. J., Yu, Y., and Zou, D. G. (2014) 3D FE static and dynamic analysis of rockfill dam with asphalt concrete
576 core. J. Dalian Univ. Technol, 54(2), 197-203.
577 Lee, J., & Fenves, G. L. (1998) Plastic-damage model for cyclic loading of concrete structures. *Journal of engineering*
578 *mechanics*, 124(8), 892-900.
579 Li, Y. long, Tang, W., Wen, L. feng, Wu, H., (2020) Dam seismic deformation evaluation method of asphalt concrete
580 core rockfill dam and its reliability analysis. *Journal of Hydraulic Engineering*, 51(5), 558–580.
581 Liu, J., Du, Y., Du, X., Wang, Z., and Wu, J. (2006) 3D viscous-spring artificial boundary in time domain. *Earthquake*
582 *Engineering and Engineering Vibration*, 5(1), 93-102.
583 Lubliner, J., Oliver, J., Oller, S., and Oñate, E. (1989) A plastic-damage model for concrete. *International Journal of*
584 *solids and structures*, 25(3), 299-326.
585 Ning Z, Liu Y, Wang W. (2021) Compressive Behavior of Hydraulic Asphalt Concrete under Different Temperatures
586 and Strain Rates. *Journal of Materials in Civil Engineering*, 2021, 33(4): 04021013.
587 Ou, Y. C., Song, J., Wang, P. H., Adidharma, L., Chang, K. C., and Lee, G. C. (2014) Ground motion duration effects

588 on hysteretic behavior of reinforced concrete bridge columns. *Journal of Structural Engineering*, 140(3), 04013065.

589 Pang, R., Xu, B., Kong, X., and Zou, D. (2018) Seismic fragility for high CFRDs based on deformation and damage

590 index through incremental dynamic analysis. *Soil Dynamics and Earthquake Engineering*, 104, 432-436.

591 Pelecanos, L., Kontoe, S., and Zdravković, L. (2020) The effects of dam–reservoir interaction on the nonlinear

592 seismic response of earth dams. *Journal of Earthquake Engineering*, 24(6), 1034-1056.

593 Pelecanos, L., Kontoe, S., and Zdravković, L. (2016) Dam–reservoir interaction effects on the elastic dynamic

594 response of concrete and earth dams. *Soil Dynamics and Earthquake Engineering*, 82, 138-141.

595 Raghunandan, M., Liel, A. B. (2013) Effect of ground motion duration on earthquake-induced structural collapse.

596 *Structural Safety*, 41, 119-133.

597 Serff, N., Seed, H. B., Makdisi, F. I., and Chang, C. Y. (1976) Earthquake-induced deformations of earth dams.

598 University of California, Berkeley.

599 Sun, B., Zhang, S., Cui, W., Deng, M., and Wang, C. (2020) Nonlinear dynamic response and damage analysis of

600 hydraulic arched tunnels subjected to P waves with arbitrary incoming angles. *Computers and Geotechnics*, 118,

601 103358.

602 Sun, B., Zhang, S., Deng, M., and Wang, C. (2020) Inelastic dynamic response and fragility analysis of arched

603 hydraulic tunnels under as-recorded far-fault and near-fault ground motions. *Soil Dynamics and Earthquake*

604 *Engineering*, 132, 106070.

605 Sun, B., Zhang, S., Deng, M., and Wang, C. (2020) Nonlinear dynamic analysis and damage evaluation of hydraulic

606 arched tunnels under mainshock–aftershock ground motion sequences. *Tunnelling and Underground Space*

607 *Technology*, 98, 103321.

608 Sun, B., Zhang, S., Deng, M., and Wang, C. (2020) Inelastic dynamic response and fragility analysis of arched

609 hydraulic tunnels under as-recorded far-fault and near-fault ground motions. *Soil Dynamics and Earthquake*
610 *Engineering*, 132, 106070.
611 Swaisgood, J. R. (2003) Embankment dam deformations caused by earthquakes. in: Pacific conference on earthquake
612 engineering (pp. pp-014).
613 Trifunac, M. D., Brady, A. G. (1975) A study on the duration of strong earthquake ground motion. *Bulletin of the*
614 *Seismological Society of America*, 65(3), 581-626.
615 Vamvatsikos, D., Cornell, C. A. (2004) Applied incremental dynamic analysis. *Earthquake Spectra*, 20(2), 523-553.
616 Wang, D. B., Liu, H. L., Yu, T., and Yang, G. (2015) Seismic fragility analysis for earth-rockfill dams based on
617 deformation. *Chinese Journal of Geotechnical Engineering*, 12(22), 54-61.
618 Wang, G., Wang, Y., Lu, W., Yan, P., and Chen, M. (2020) Earthquake Direction Effects on Seismic Performance of
619 Concrete Gravity Dams to Mainshock–Aftershock Sequences. *Journal of Earthquake Engineering*, 24(7), 1134-1155.
620 Wang, G., Wang, Y., Zhou, W., and Zhou, C. (2015) Integrated duration effects on seismic performance of concrete
621 gravity dams using linear and nonlinear evaluation methods. *Soil Dynamics and Earthquake Engineering*, 79, 223-
622 236.
623 Wang, G., Zhang, S., Wang, C., and Yu, M. (2014) Seismic performance evaluation of dam-reservoir-foundation
624 systems to near-fault ground motions. *Natural hazards*, 72(2), 651-674.
625 Wang, W., Höeg, K. (2016) Simplified material model for analysis of asphalt core in embankment dams. *Construction*
626 *and Building Materials*, 124, 199-207.
627 Wang, W., Höeg, K., and Zhang, Y. (2010) Design and performance of the Yele asphalt-core rockfill dam. *Canadian*
628 *geotechnical journal*, 47(12), 1365-1381.
629 Wang, Z. Z., Jiang, Y. J., and Zhu, C. A. (2019) Seismic energy response and damage evolution of tunnel lining

structures. *European Journal of Environmental and Civil Engineering*, 23(6), 758-770.

Xu, B., Pang, R., and Zhou, Y. (2020) Verification of stochastic seismic analysis method and seismic performance evaluation based on multi-indices for high CFRDs. *Engineering Geology*, 264, 105412.

Zhang, S., Wang, G., Pang, B., Du, C. (2013) The effects of strong motion duration on the dynamic response and accumulated damage of concrete gravity dams. *Soil Dynamics and Earthquake Engineering*, 45, 112-124.

Zhu-Jiang, S. H. E. N., and Gang, X. U. (1996) Deformation behavior of rock materials under cyclic loading. *Journal of Nanjing Hydraulic Research Institute*, 2, 143-150.

Figures

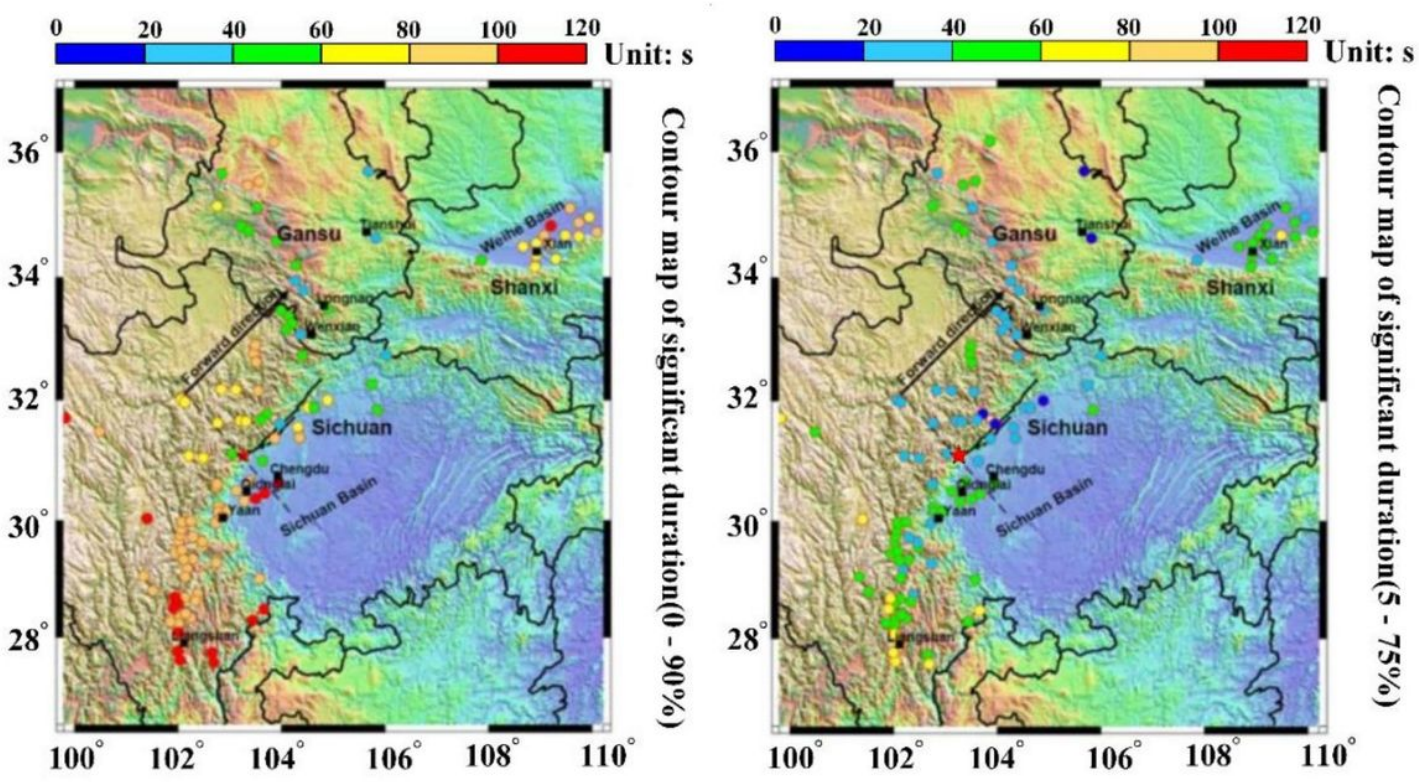

Figure 1

Spatial distribution of significant duration recorded from Wenchuan earthquake (Mw7.9, 2008). (a) 0-90% significant duration; (b) 5-75% significant duration. Note: The designations employed and the presentation of the material on this map do not imply the expression of any opinion whatsoever on the part of Research Square concerning the legal status of any country, territory, city or area or of its authorities, or concerning the delimitation of its frontiers or boundaries. This map has been provided by the authors.

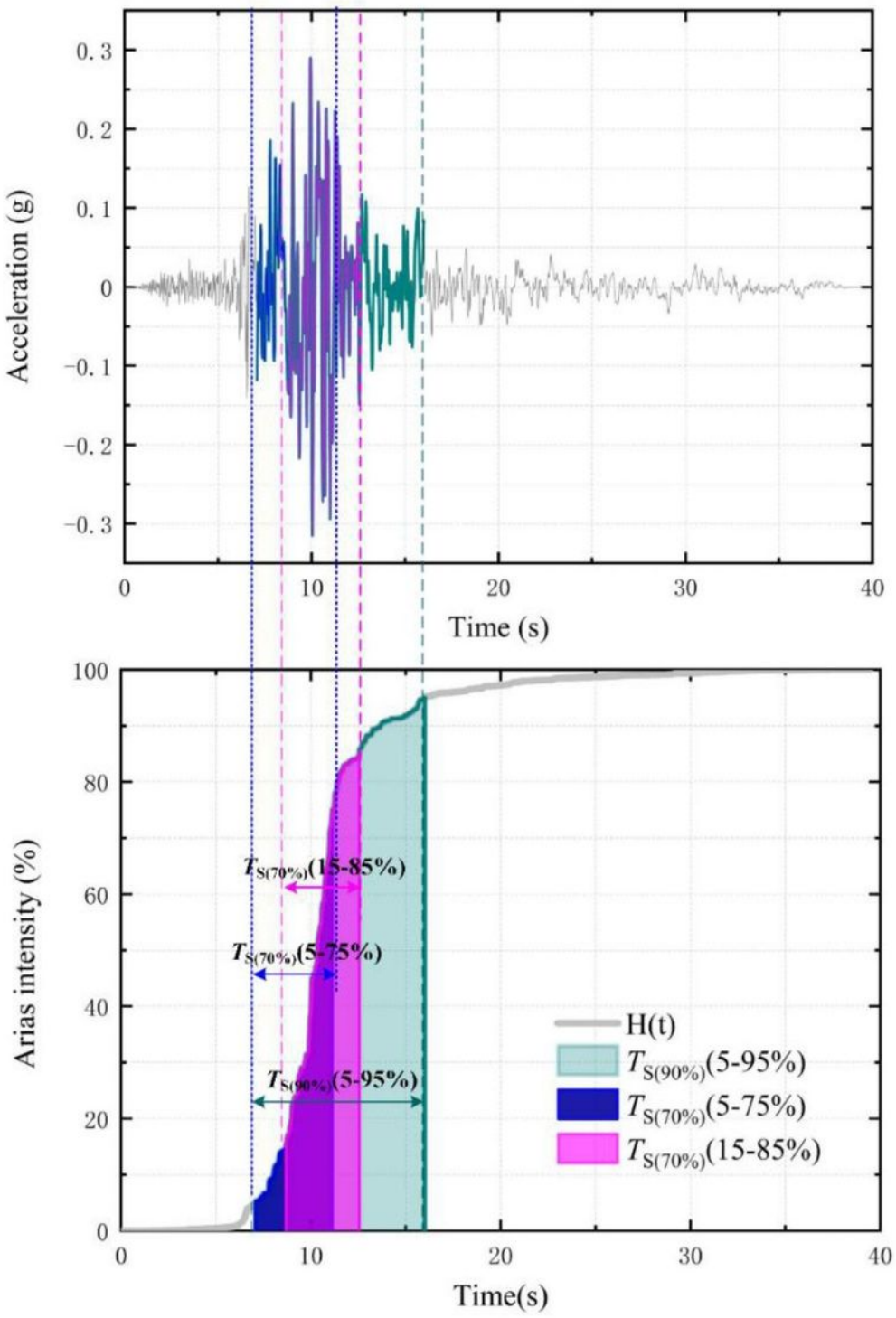

Figure 2

The husid diagram of three SDs of an as-record accelerogram.

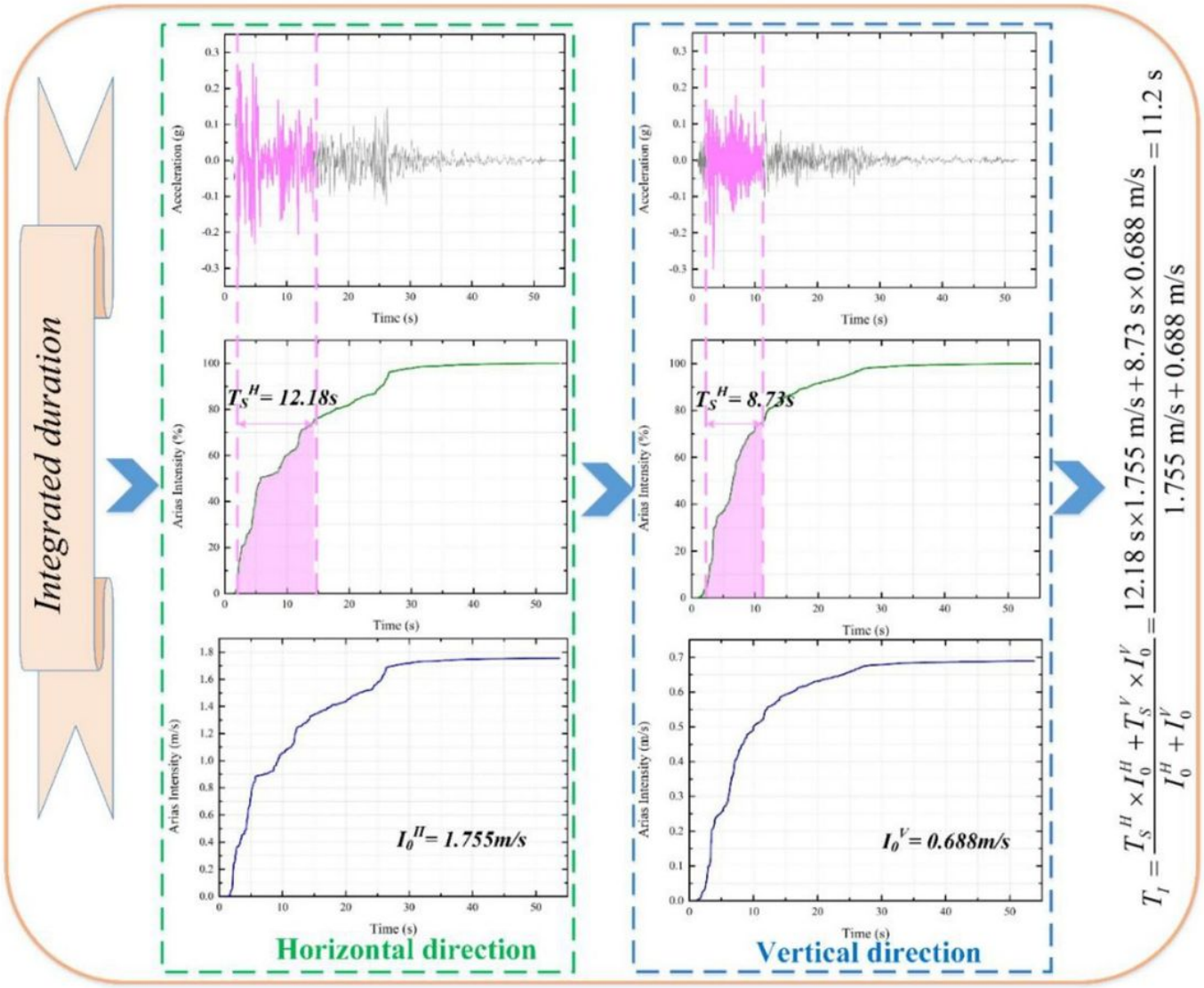

Figure 3

Calculation progress of ID based on SD (5-75%).

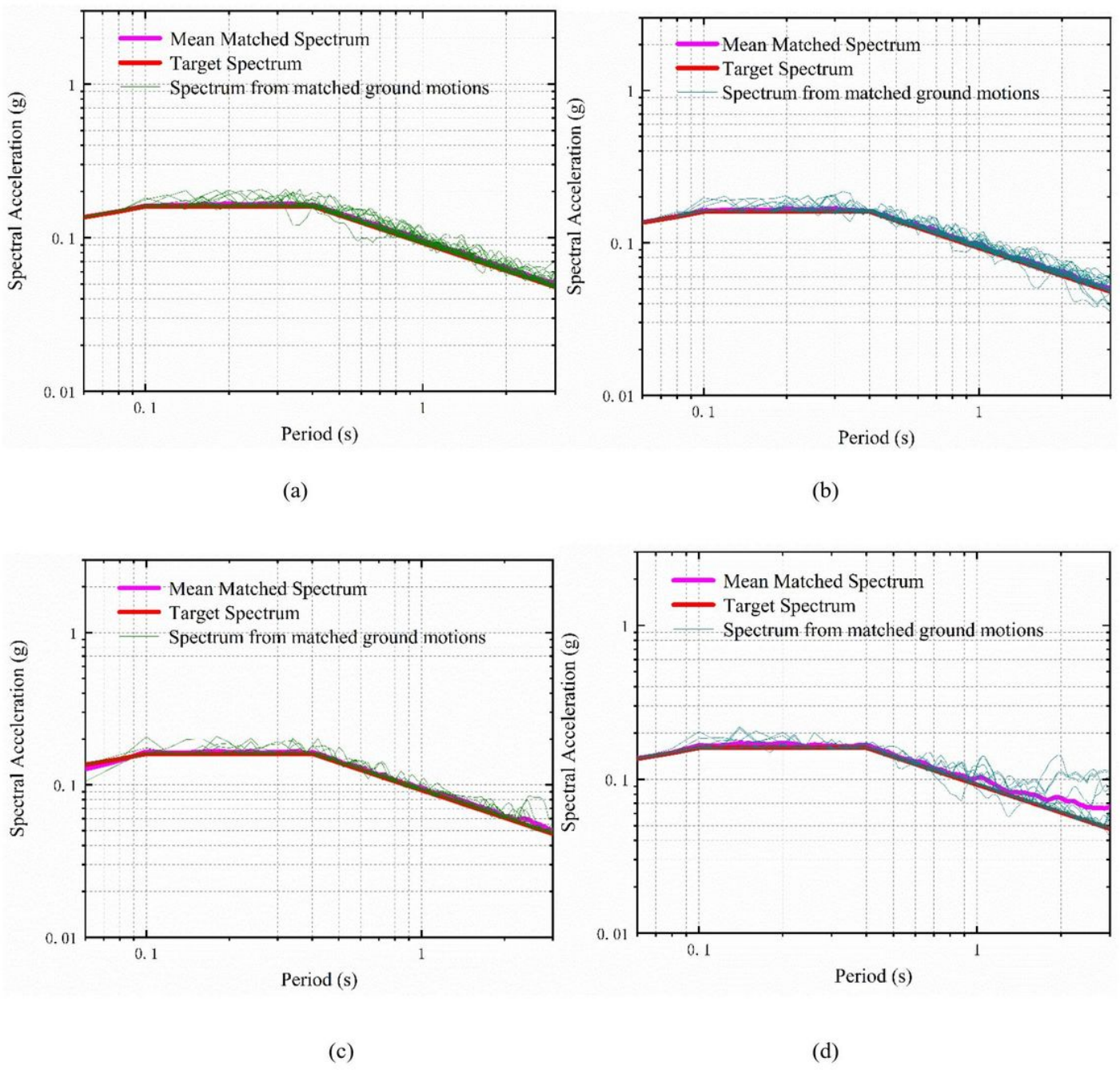

Figure 4

Comparison of the adjusted response spectra of short - and long – duration GMs: (a) horizontal short – duration; (b) vertical direction short – duration; (c) horizontal long – duration; (b) vertical direction long – duration.

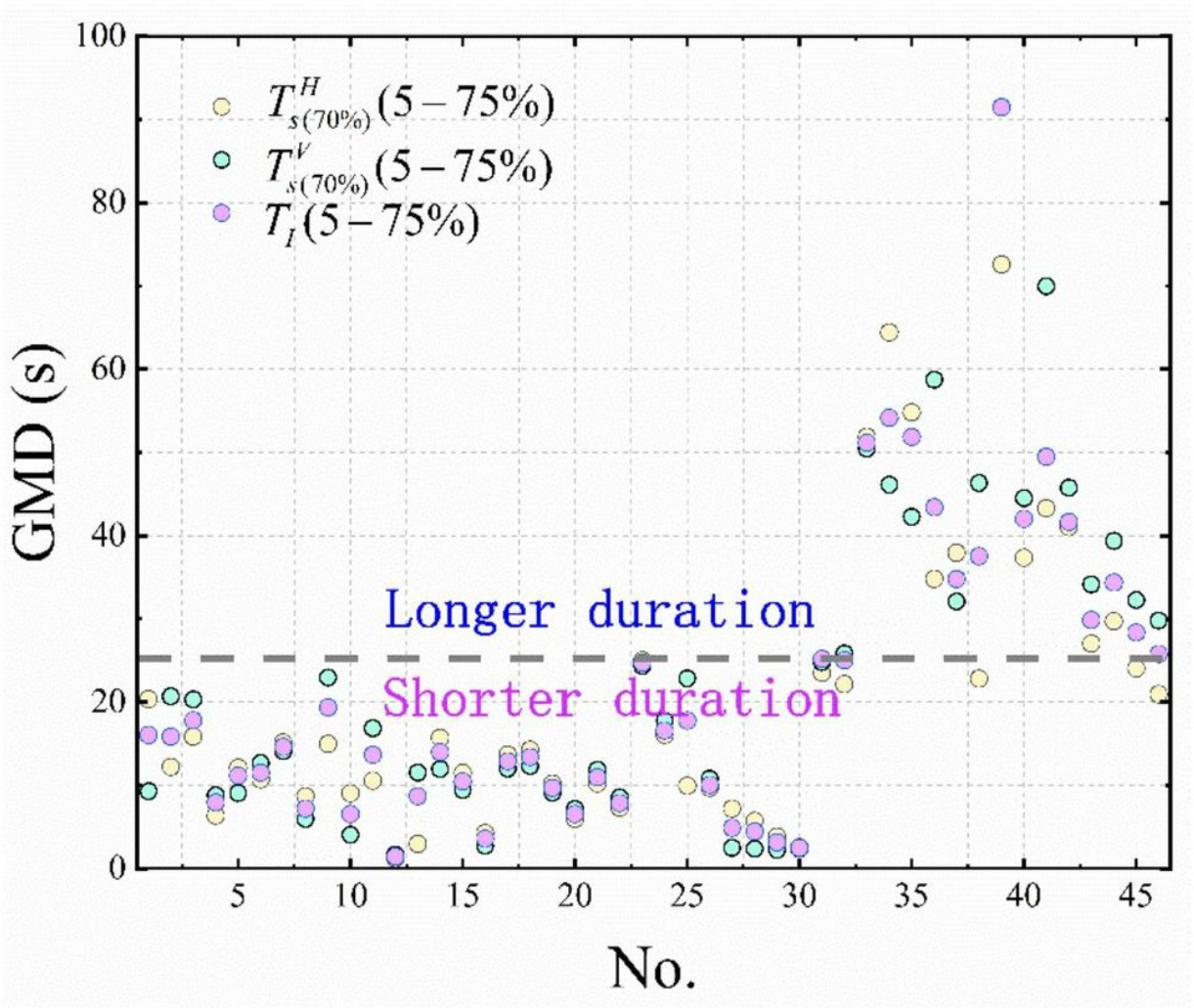

Figure 5

Distribution of GMD in database after matching spectral acceleration.

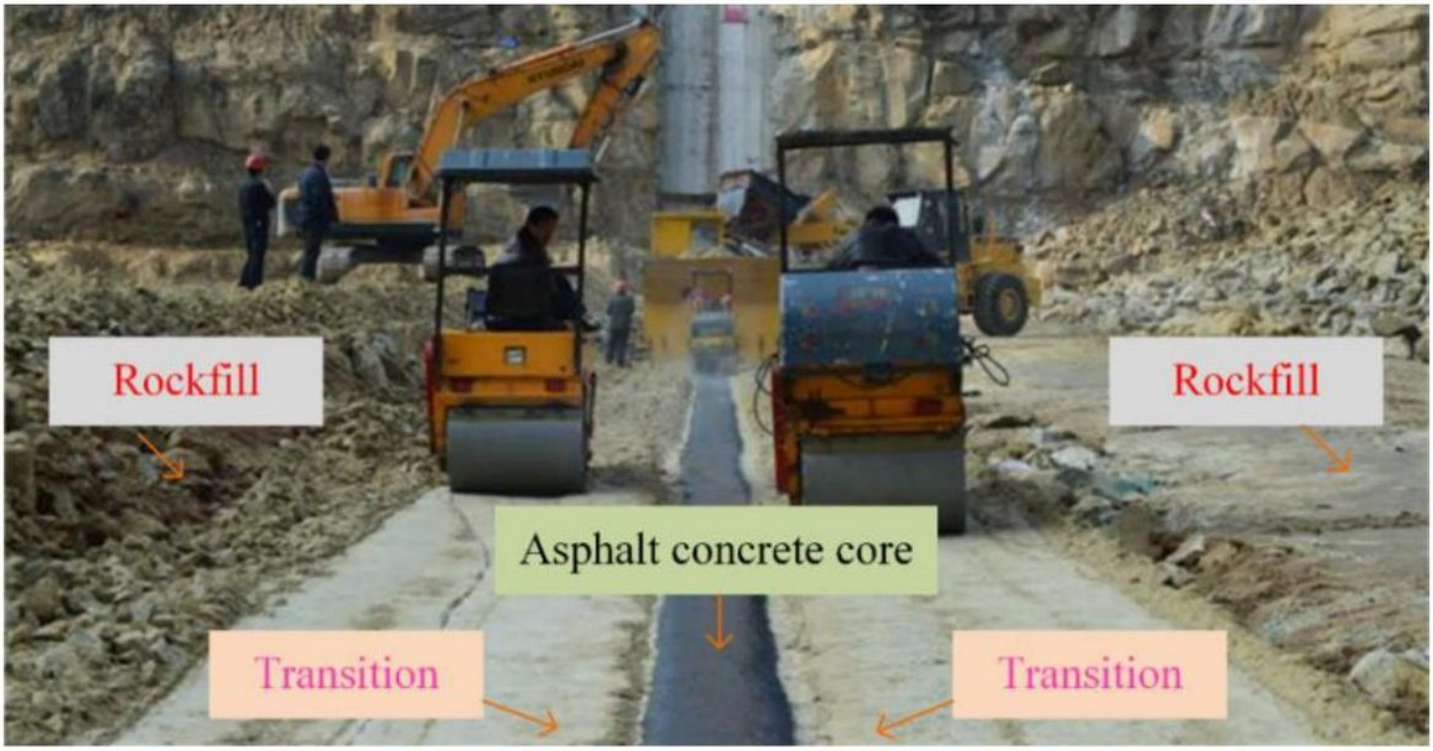

Figure 6

Construction of high ACCRD.

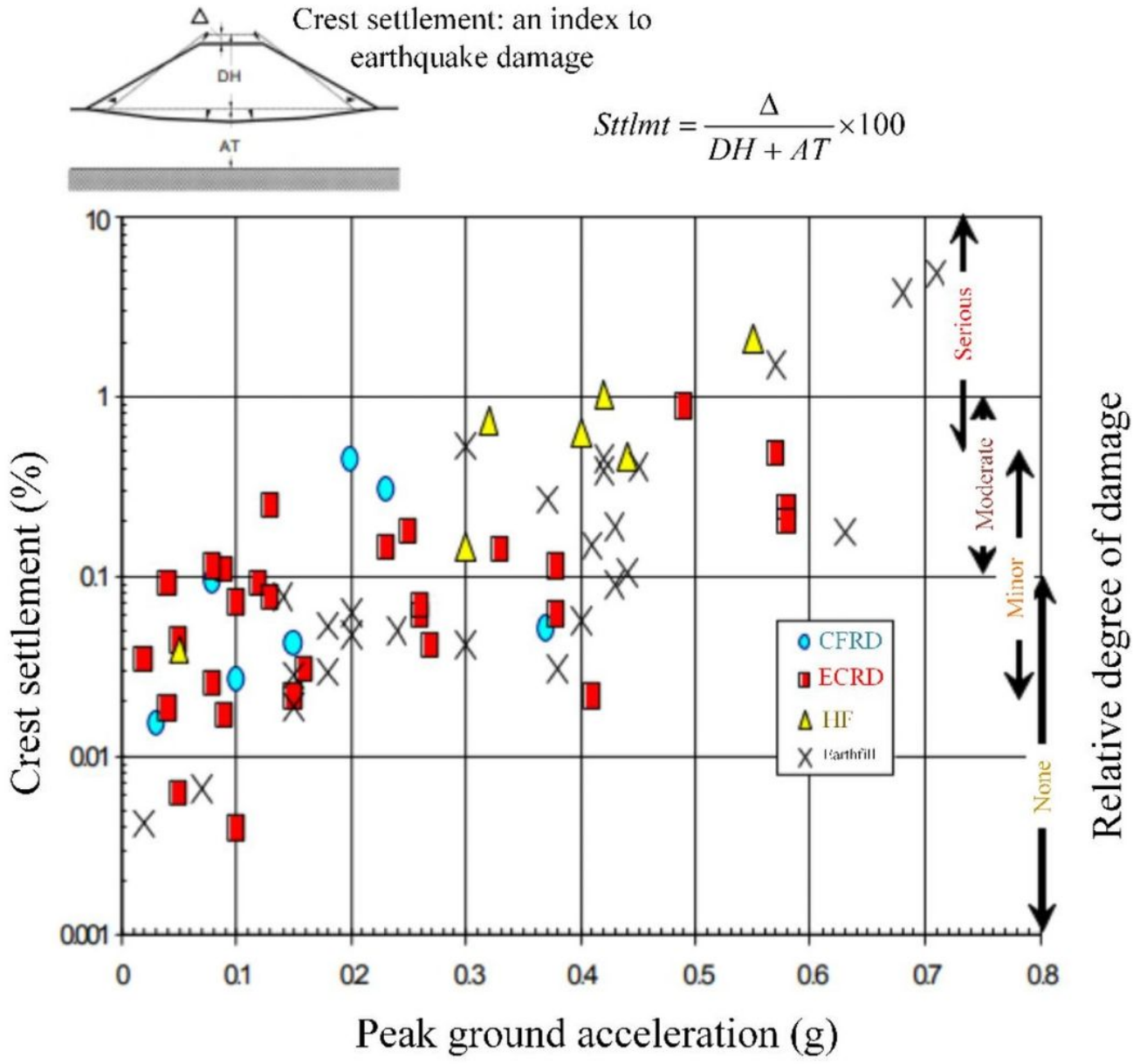

Figure 7

Construction of high ACCRD.

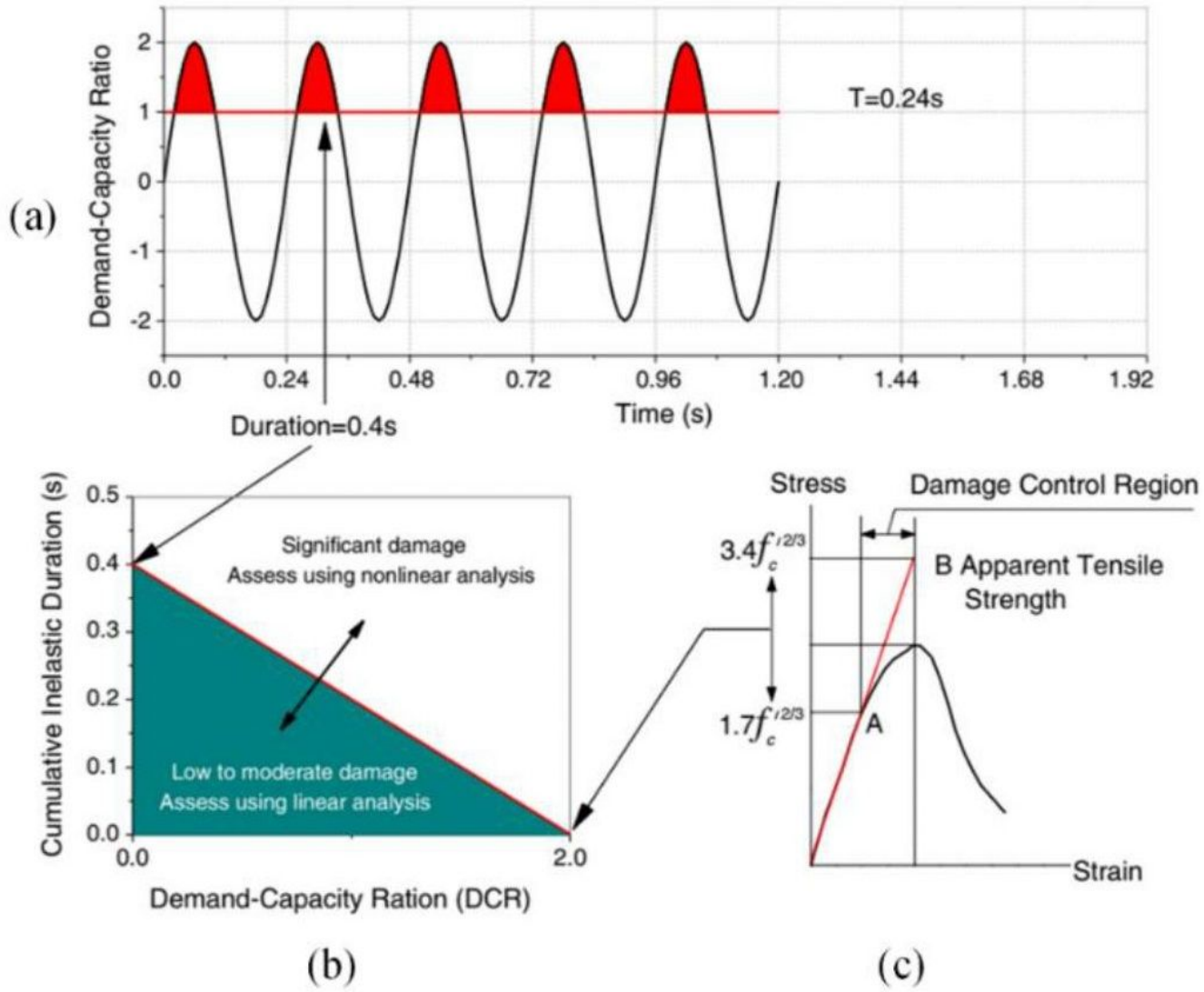

Figure 8

Illustration of seismic performance and damage criteria (Ghanaat, 2004).

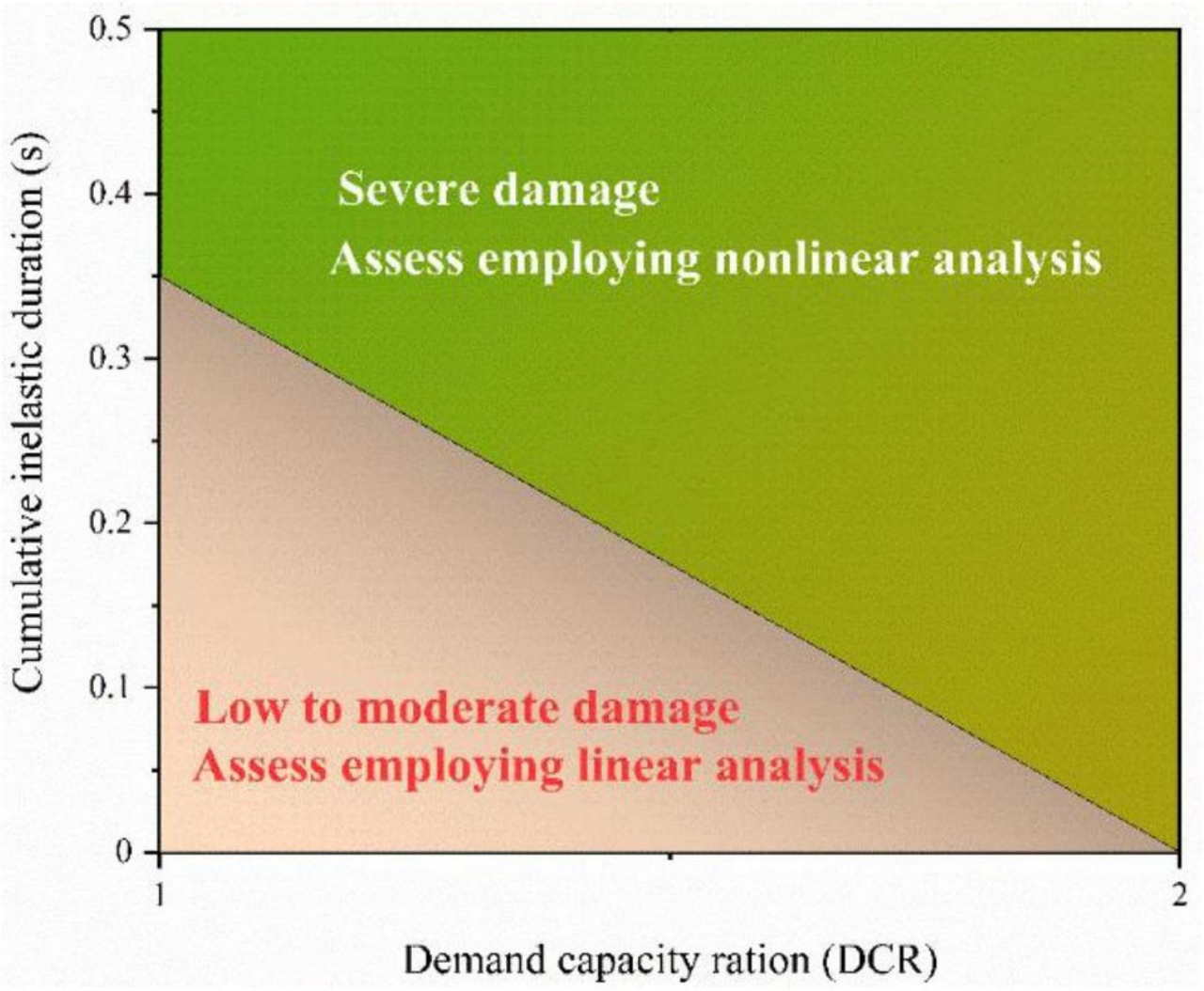

Figure 9

Seismic performance and limit state threshold value of asphalt concrete core.

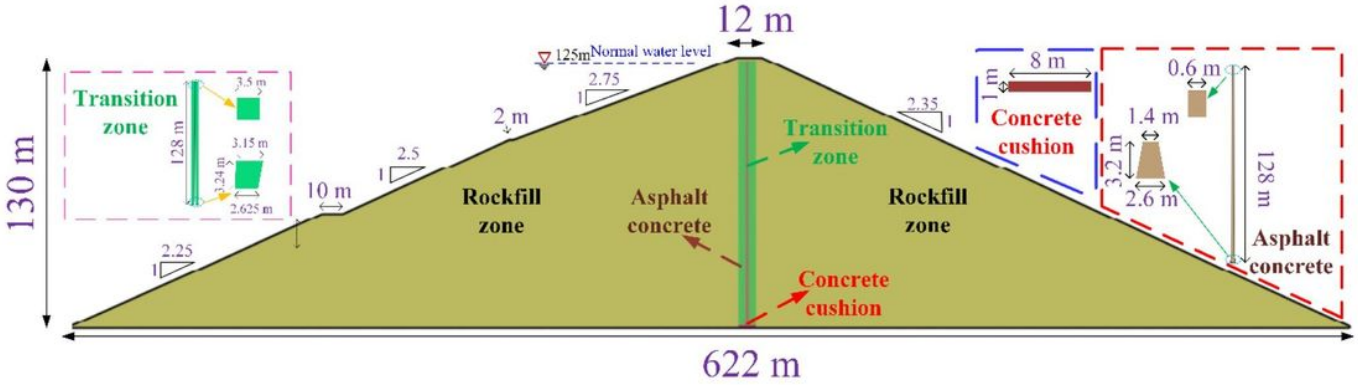

Figure 10

Construction and design of Dashimen dam: (a) aerial view; (b) cross section

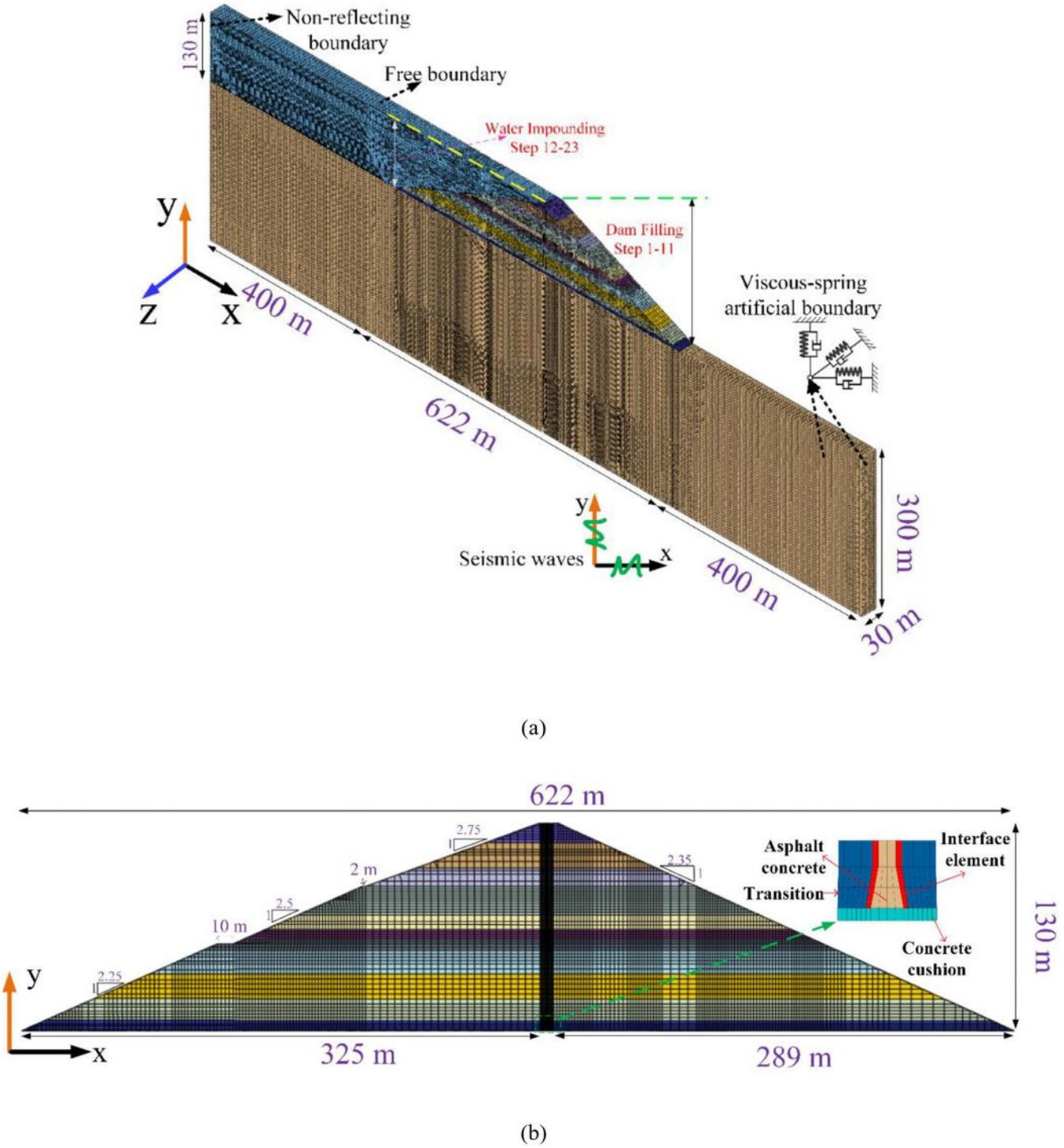

Figure 11

Details of the high ACCRD – water – foundation FE model.

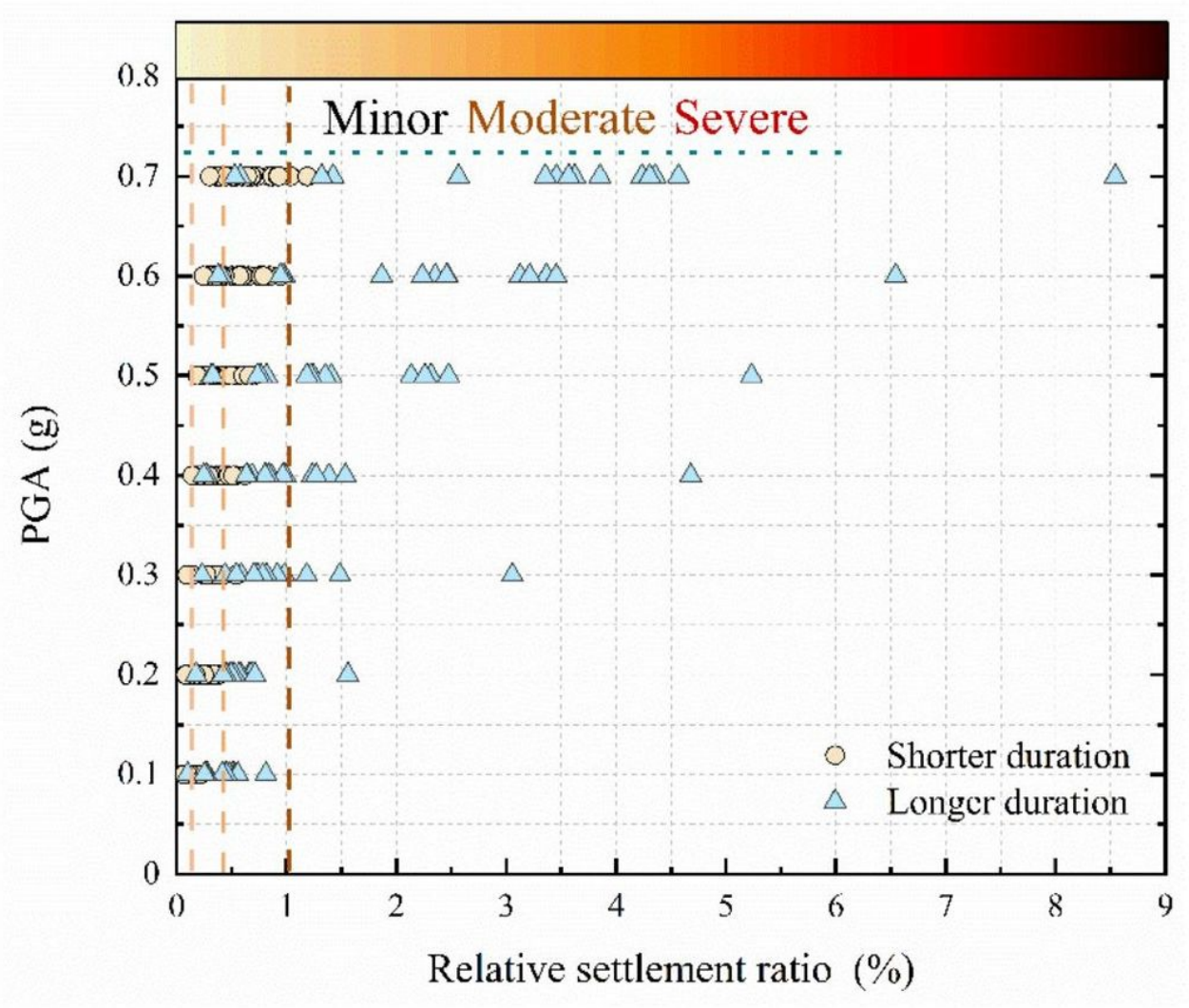

Figure 12

The RSR of multiple strip response under different seismic intensities.

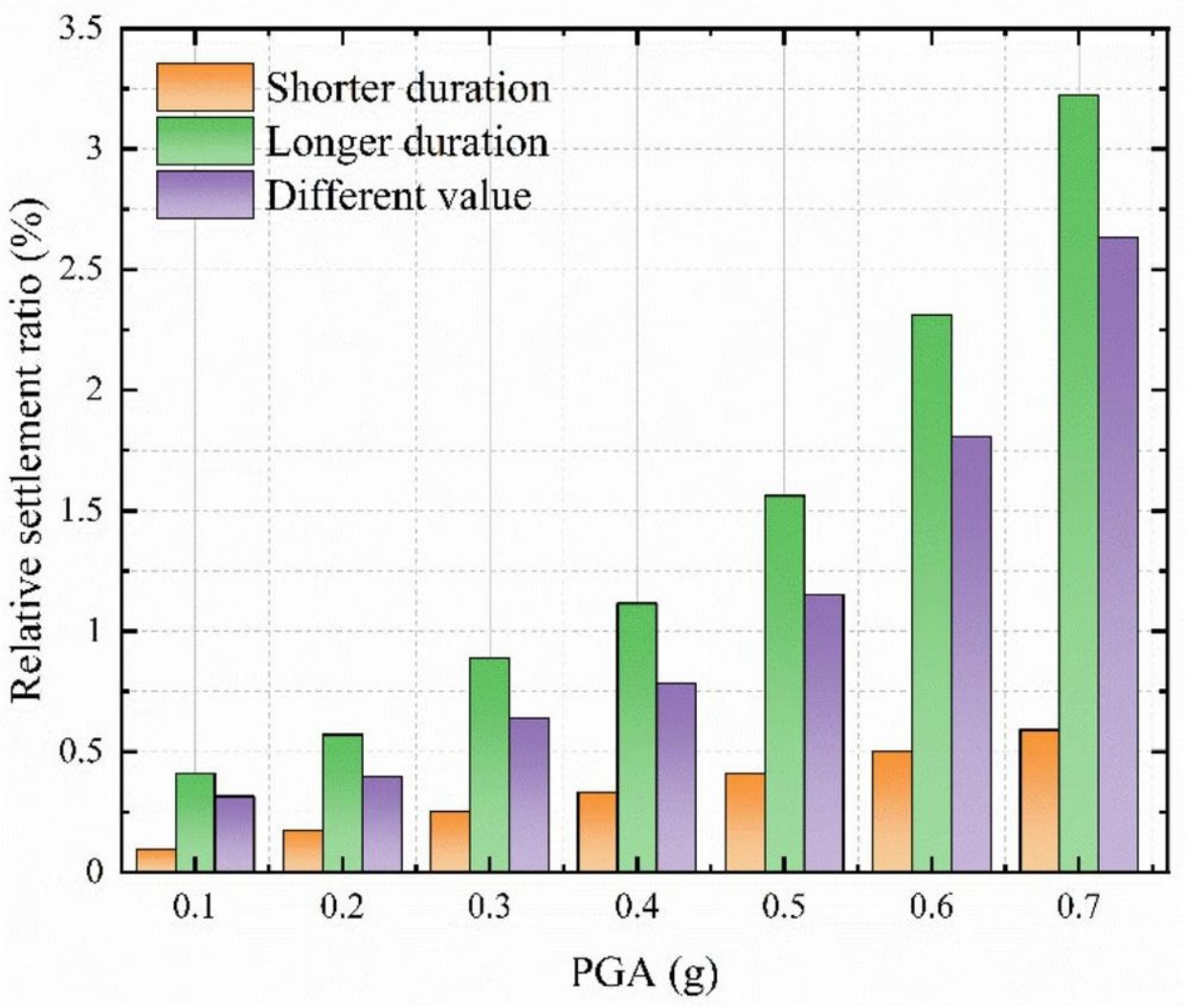

Figure 13

Mean value of RSR.

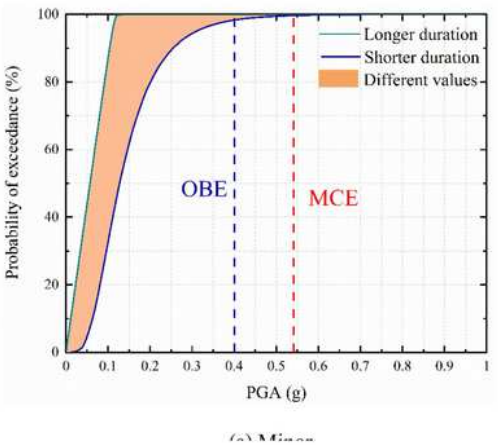

(a) Minor

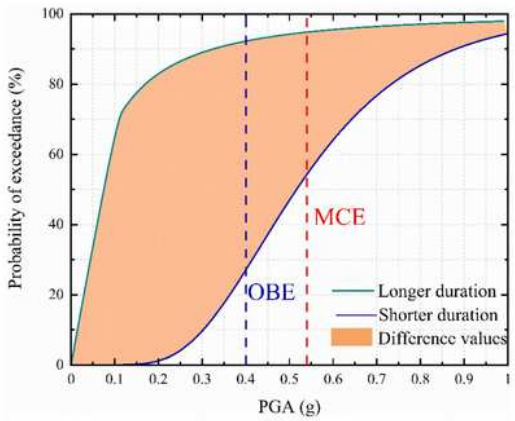

(b) Moderate

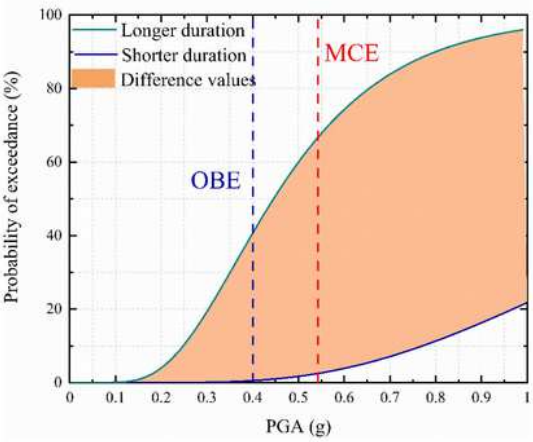

(c) Severe

Figure 14

Comparison of fragility curves of short - and long - duration GMs for different performance levels: (a) Minor damage. (b) Moderate damage, and (c) Severe damage.

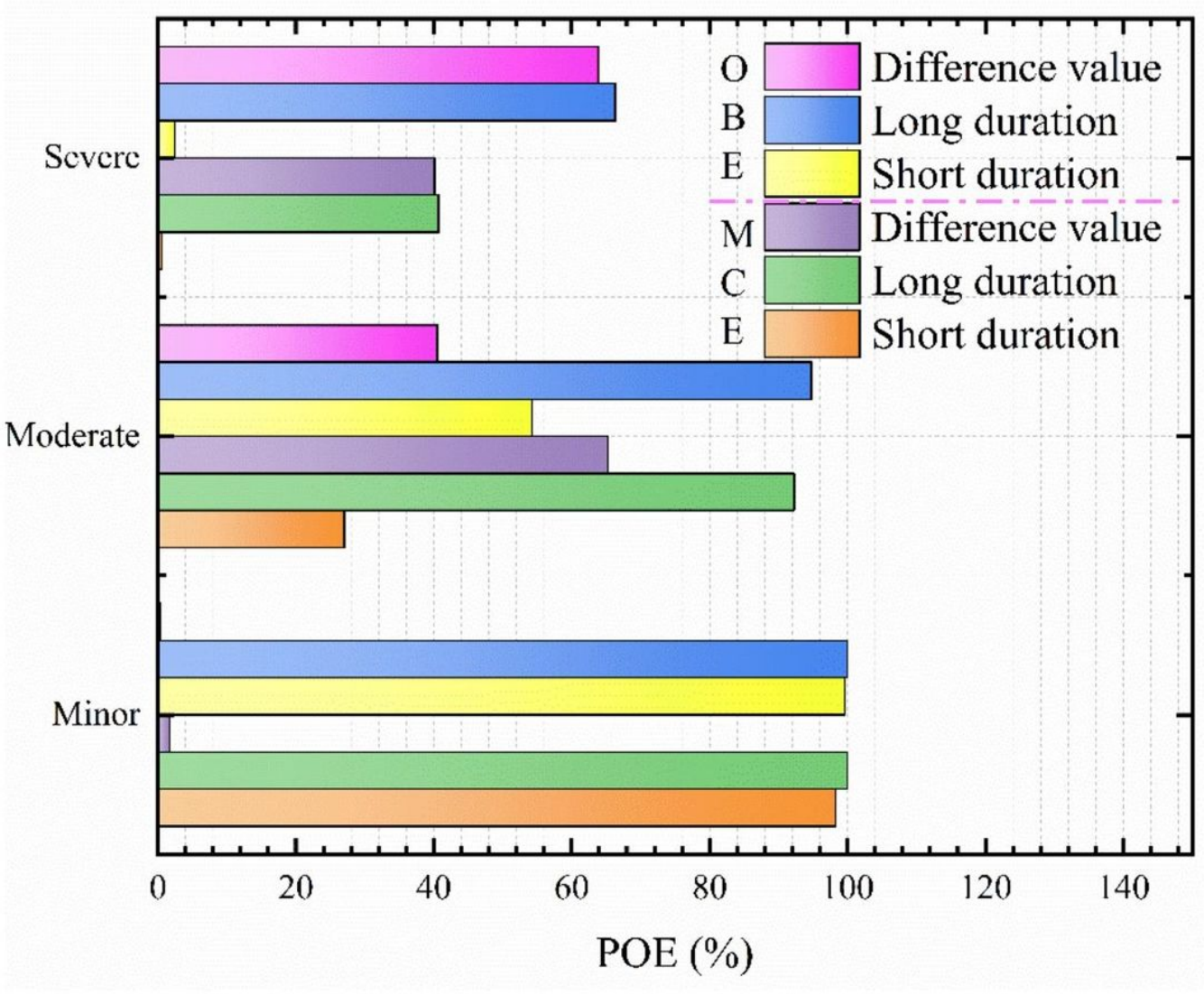

Figure 15

The POE of different performance levels of RSR under OBE and MCE.

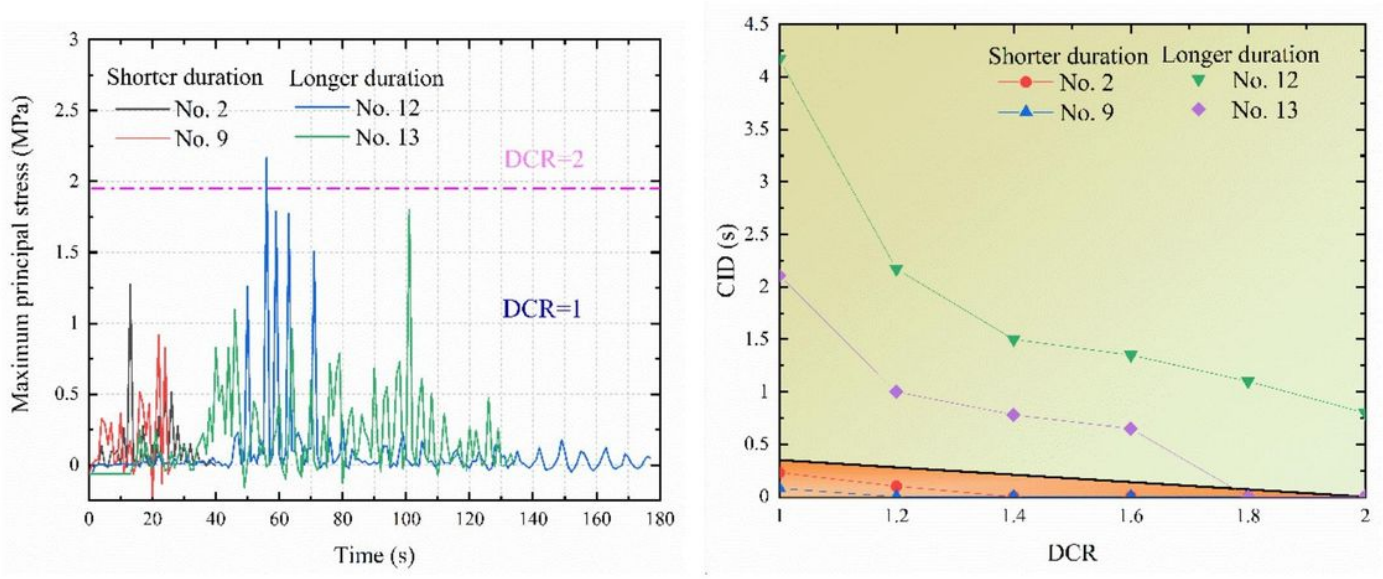

(a) Time histories of maximum principal stress (b) Performance assessment curves

Figure 16

Time histories of maximum principal stress and performance assessment curves for short - and long - duration GMs with a PGA level of 0.5g.

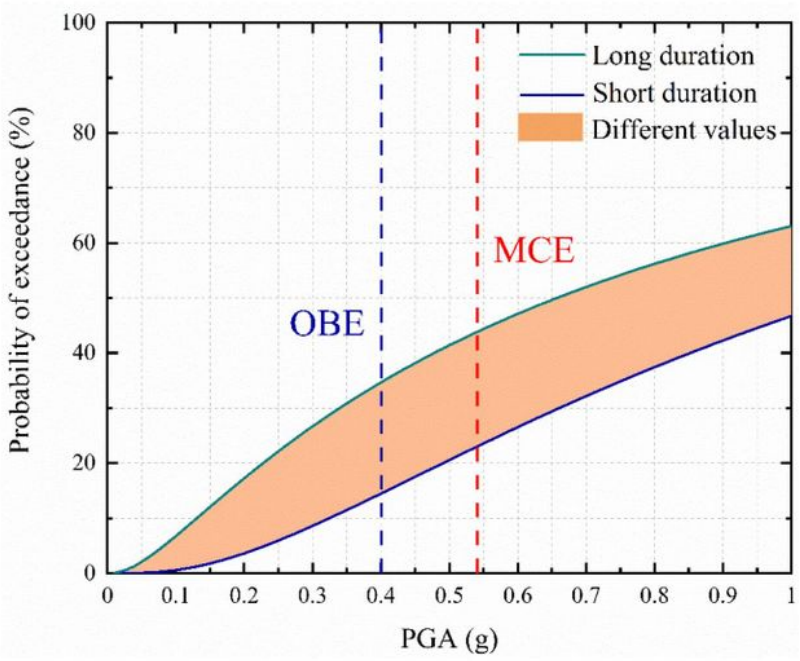

(a) Moderate

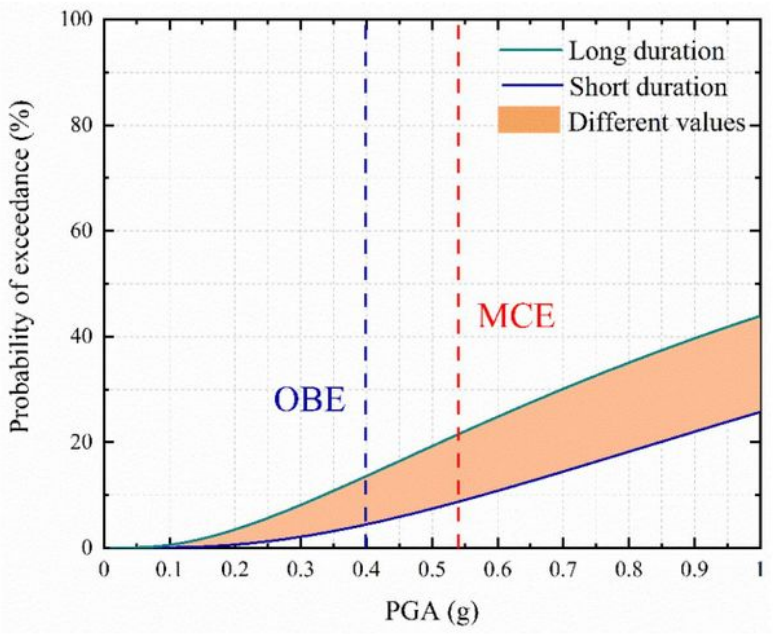

(b) Severe

Figure 17

Seismic fragility curves with short - and long - duration GMs for (a) moderate; (b) severe.

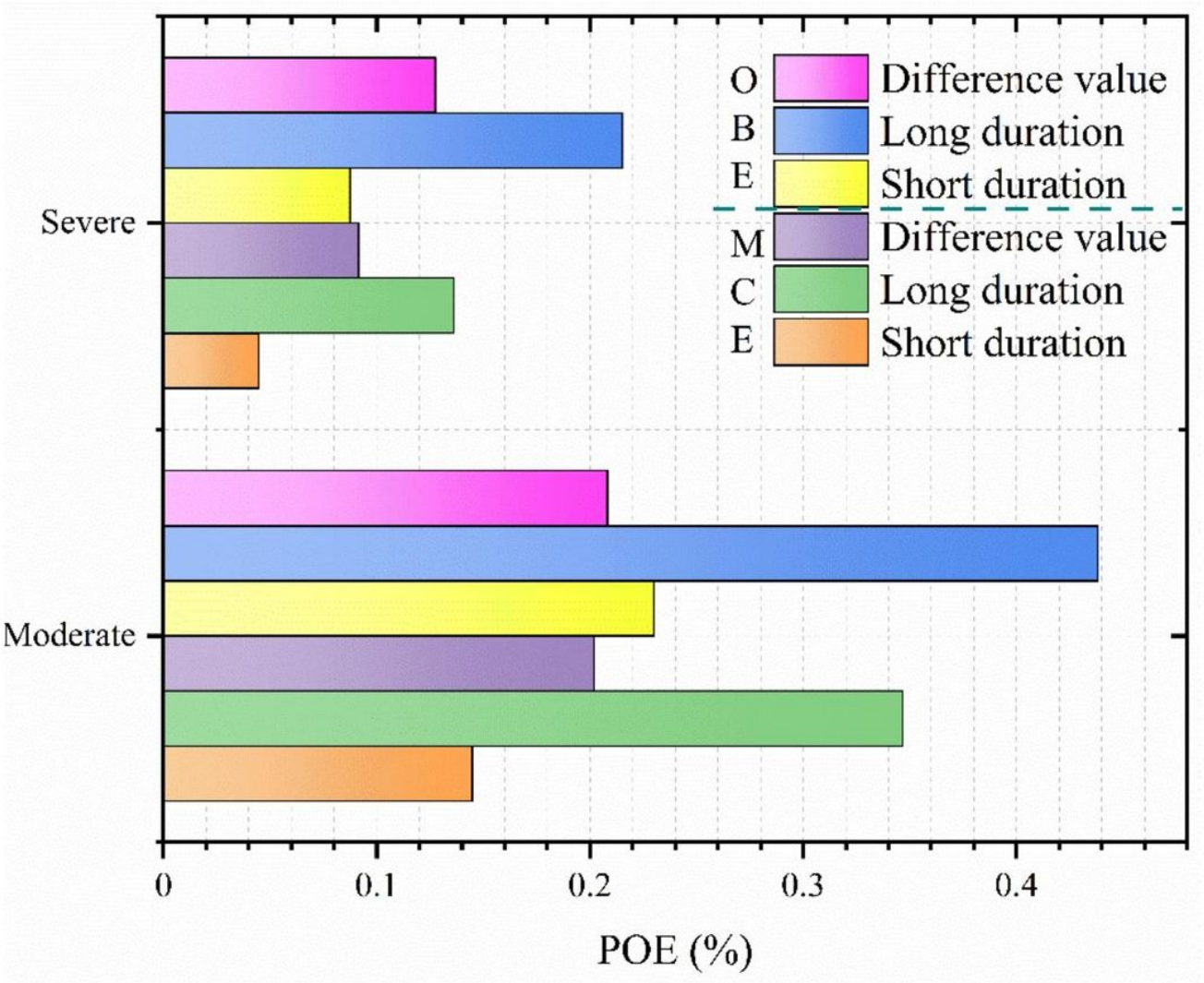

Figure 18

The POE of different performance levels of RSR under OBE and MCE.